Medical Image Analysis 65 (2020) 101773

Contents lists available at ScienceDirect

Medical Image Analysis

journal homepage: www.elsevier.com/locate/media

Detection, segmentation, simulation and visualization of aortic dissections: A review

Antonio Pepe[a,b,c,d,1,*], Jianning Li[a,c,d,1,*], Malte Rolf-Pissarczyk[d,e], Christina Gsaxner[a,c,d,f], Xiaojun Chen[g], Gerhard A. Holzapfel[d,e,h], Jan Egger[a,c,d,f,g,*]

[a] Institute of Computer Graphics and Vision, Graz University of Technology, Inffeldgasse 16, 8010 Graz, Austria
[b] Stanford University, School of Medicine, Department of Radiology, 291 Campus Drive, Stanford, CA 94305, USA
[c] Computer Algorithms for Medicine Laboratory, Graz, Austria
[d] BioTechMed-Graz, Mozartgasse 12/II, 8010 Graz, Austria
[e] Institute of Biomechanics, Graz University of Technology, Stremayrgasse 16-II, 8010 Graz, Austria
[f] Department of Oral and Maxillofacial Surgery, Medical University of Graz, Auenbruggerplatz 2, 8036 Graz, Austria
[g] Shanghai Jiao Tong University, School of Mechanical Engineering, 800 Dong Chuan Road, Shanghai 200240, China
[h] Norwegian University of Science and Technology (NTNU), Department of Structural Engineering, 7491 Trondheim, Norway

ARTICLE INFO

Article history:
Received 12 November 2019
Revised 1 June 2020
Accepted 6 July 2020
Available online 7 July 2020

MSC:
74L15
92C55
94A08
62P10

Keywords:
Aorta
Dissection
Detection
Segmentation
Visualization
Simulation
Computed tomography

ABSTRACT

Aortic dissection (AD) is a condition of the main artery of the human body, resulting in the formation of a new flow channel, or false lumen. The disease is usually diagnosed with a computed tomography angiography scan during the acute phase. A better understanding of the causes of AD requires knowledge of the aortic geometry (segmentation), including the true and false lumina, which is very time-consuming to reconstruct when performed manually on a slice-by-slice basis. Hence, different automatic and semi-automatic medical image analysis approaches have been proposed for this task over the last years. In this review, we present and discuss these computing techniques used to segment dissected aortas, also in regard to the detection and visualization of clinically relevant information and features from dissected aortas for customized patient-specific treatments.

1. Introduction

The aorta is the main artery of the human body and carries oxygen-rich blood from the heart to the rest of the body through its branch arteries. On a microscale level, the aortic wall consists of three layers – intima, media, and adventitia – which primarily consist of collagen fibers, elastic fibers, vascular smooth muscle cells and the ground substance. A dissection of the aorta is defined as a separation of layers of the aortic wall, causing blood to flow into a new cavity, which is called 'false' lumen, to distinguish it from the physiological 'true' lumen of the aorta; see Fig. 1 and Fig. 2 for illustrations and Sherifova and Holzapfel (2019) for a recent review.

An aortic dissection (AD) is often initiated from an intimal tear (Thubrikar et al. (1991)) or from a perforation of the intima caused by intramural hemorrhage and hematoma formation (Khan and Nair (2002)). According to the Stanford classification (LeMaire and Russel (2011)), AD can be classified according to the origin of the intimal tear: if the ascending aorta is involved, then it is classified as Type A (Type A aortic dissection – TAAD), otherwise, if only the arch or the descending aorta are involved, it is classified as Type B (Type B aortic dissection – TBAD). According to a previous study (Tsai et al. (2007)), we can summarize the typical development of TBAD as the following six stages:

- Stage 1: The patient has aortic tissue abnormalities or increased aortic wall stress

* Corresponding authors.
E-mail addresses: antonio.pepe@tugraz.at (A. Pepe), jianning.li@icg.tugraz.at (J. Li), jan.egger@medunigraz.at (J. Egger).
[1] Joint first authors

https://doi.org/10.1016/j.media.2020.101773
1361-8415/

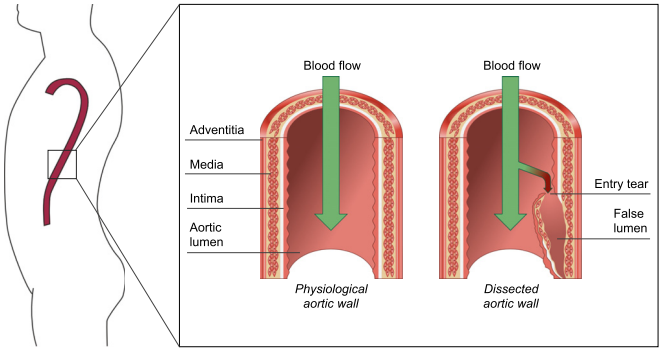

Fig. 1. Computer-generated visualization of the aortic wall, of its different layers, and of its deformation due to the formation of a primary entry tear.

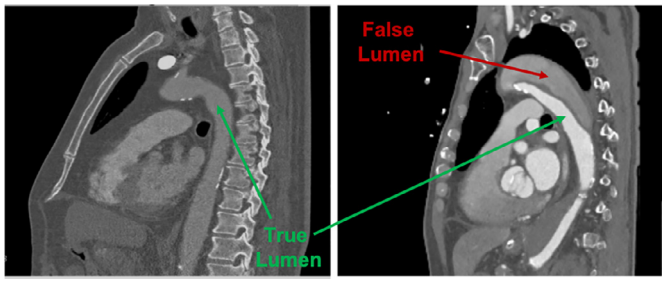

Fig. 2. Computed tomography angiography of a healthy subject (left), where only one lumen is visible in the aorta; an aortic dissection case, where the false and true lumina are clearly distinguishable (right).

- Stage 2: Due to an intimal tear, a small false lumen forms, but the effect on the blood flow is still minimal
- Stage 3: The false lumen propagates downstream in the longitudinal direction, but without a thrombosis; the blood flow is disturbed due to the presence of the false lumen
- Stage 4: The false lumen reaches its final shape. A second or more distal tear may occur. The blood flows freely through the false and true lumina once the additional distal tears occur
- Stage 5 (optional): A thrombosis accumulates from the distal side of the false lumen. The distal tears may gradually be blocked by the thrombus
- Stage 6 (optional): Complete thrombus is formed in the false lumen. The blood pressure within the false lumen is very low and non pulsatile

It should be mentioned that the false lumen might never develop a thrombus, and hence the stages 5 and 6 may not occur in a patient. The factors causing the formation of a thrombus are still investigated and prediction models have been suggested, see, e.g., Menichini et al. (2016).

A quantitative and accurate analysis of all these stages is a non-trivial task due to the significant shape changes which affect the aorta. Therefore, to model and quantify the progression of the disease, different segmentation techniques have been proposed, which automatically or semi-automatically segment the volume of the dissected aorta, and provide a semantic representation of the true lumen, the false lumen, the aortic wall and the intimal flap. In this paper, we first provide an overview of the clinical workflow, including its current implications, and afterwards we review the different approaches which have been suggested, discussing their strengths and limitations in regard to computational complexity, segmentation accuracy, data requirements and the amount of user interaction.

Manuscript Outline We present a review on the fundamental technologies used in computer-aided diagnosis and treatment of AD which includes AD segmentation, detection, visualization, simulation and detection of the intimal tear. We review AD segmentation papers which have the goal to segment the aortic lumen, i.e. the true lumen and the false lumen together. These papers, which pursue this topic, we address as *core papers* in this review. In Section 2 we describe AD segmentation as the core step for computer-aided diagnosis, 3D visualization, simulation of the hemodynamics and further AD-specific analyses such as the measurement of aortic diameters for surgery planning and follow-up. The core papers are thoroughly analysed in Section 3. Further *non-core papers*, covering intimal flap segmentation, AD detection, intimal tear detection, visualization and simulation are covered in Section 4. We name these papers as *additional papers* as they are usually dependent on the task of the AD segmentation. Eventually, we conclude this review with Section 5, with a summary of the current state of AD segmentation methods and provide an outlook for future development of automatic AD segmentation approaches. The logic behind this arrangement of the review is that improved AD segmentation will concurrently benefit AD-related applications, ranging from detection to visualization and simulation. For clarification, it is worth to note that a paper that is focused only on the segmentation of the aortic lumen is still categorized as *core paper*. The reason behind this choice was that the paper is a prelude to further research published by the same research group. The group later on published follow-up research on the segmentation of the true and false lumina. Furthermore, even if the segmentation of the intimal flap is sometimes an intermediate step in the AD segmentation, we categorize these papers as *additional papers* in Section 4, as the papers did not explicitly address the topic of aortic lumen segmentation.

Search Strategy We performed a search in IEEE Xplore Digital Library, Scopus, DBLP, PubMed, and Google Scholar for the keyword *'aortic dissection'* together with any keyword between {*'segmentation', 'detection', 'visualization', 'mesh', 'geometry'*}. During the search we retrieved 1 328 non-distinct records. Additionally, we considered three papers, which were already known to us. Based on the titles and abstracts, we excluded all the records with only clinical contributions such as radiological findings (e.g., Kim et al. (2019)). After this stage, we assessed the resulting 99 distinct papers and excluded 63 of them. The reason for exclusion has most commonly been either the overlap of content with other papers or the usage of AD in the abstract and introduction as motivation, but lack of objective results and discussion on AD images. This resulted in a total of 7 *core papers* about AD segmentation, which will be covered in-depth in our review. However, we excluded papers not written in English and non peer-reviewed manuscripts and reports. To the best of our knowledge, this is the first review that gives a thorough analysis of all the published AD segmentation studies. In addition, we provide a qualitative synthesis of papers regarding the detection, visualization, and simulation of AD and the segmentation of the intimal flap. We will refer to these papers as *additional papers*. The number of these *additional papers* is 29, including three AD segmentation, seven intimal flap segmentation, five AD detection, one intimal tear detection, four AD visualization and nine simulations. An overview of these papers is summarized in Fig. 3. Note that we did not include all the existing published research for the *additional papers*, and only the most recent, representative papers were considered. However, we attempted to make sure that the selected papers cover all the methodologies for each topic. More information on the search strategy and the identified papers can be found in the section on 'Supplementary Material'.

2. AD Segmentation: Clinical workflow, implication and relevance

A personalized and precise management of AD has been increasingly desired in thoracic endovascular aortic repair (TEVAR)

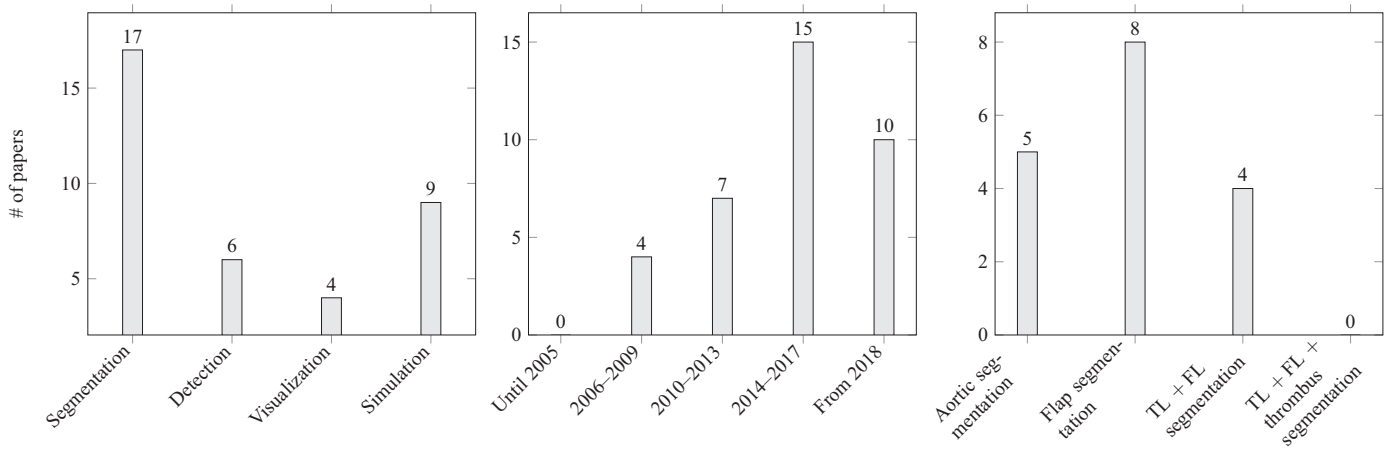

Fig. 3. Categorization by numbers of related AD publications presented and discussed in the present review, similar to the review article about generative adversarial networks of Yi et al. (2019). The leftmost diagram shows the overall number of papers according to the different tasks, i.e. segmentation, detection, visualization and simulation. A detailed list of these papers is provided in Table 1 and Table 2. The diagram in the middle presents the total amount of publications according to the year they were published. Instead of showing the publications per year, we chose five categories to provide a more compact view. The three bars in the middle show always a time frame of four years. The first and last bars show the number of publications until 2005 and from 2018 on. Finally, the rightmost diagram displays the number of publications that segment the aorta, the intimal flap, the true (TL), the false lumen (FL), and the TL, FL and the thrombus. Note that the segmentation is often the very first step in an overall medical image processing pipeline, and all subsequent steps depend on it.

(Krol and Panneton (2017)). Such a scheme can be involved in all stages of AD management, including preoperative planning, follow-up, prognosis and prediction of the long-term outcome. During surgical planning, it is crucial to select and place the stent-graft based on the geometrical characteristics of the patient's aorta, similarly to aortic aneurysms (Egger et al. (2012)), such as diameters, volumetric shape and, for dissections (Wang and Fairman (2009)), the exact location of the intimal tear – information, which has shown to be effective in reducing complication and recurrence rates (Dake et al. (1999); Huang et al. (2013); Nienaber et al. (2013); Rohlffs et al. (2015)). Although not yet standardized, a crucial reason for these *patient-specific* stent-grafts is to prevent so-called 'endoleaks' (Lu et al. (2015)), and, therefore, avoid a re-intervention due to a disconnection between the stent-graft and the aortic wall (Parmer et al. (2006)).

During follow-up, an evaluation of the dissection development is required for vascular surgeons to assess the effect of TEVAR on the patient, which includes observing the changes in diameter, volume and morphology of true and false lumina (Schoder et al. (2007); Huptas et al. (2009); Kim et al. (2011); Melissano et al. (2012)). These geometrical characteristics of ADs are important prognostic factors, also in AD management. Aided by commercial software, such as Aquarius (https://www.terarecon.com/, TeraRecon, Foster City, CA) and 3Mensio (https://www.3mensio.com/), vascular surgeons can obtain a 3D model of the dissected aorta for morphological evaluation, manually segment (identify) true lumen and false lumen for diameter and volume measurement and locate the intimal tear by examining the computed tomography angiography (CTA) image in a slice-wise manner (Stanley et al. (2011); Qing et al. (2012); Codner et al. (2019)). Although commercial applications support surgeons and radiologists covering these tasks, to the best of our knowledge, they still require an intense user interaction, which results in time-consuming and error-prone operations, with a remarkable user dependability. Furthermore, it remains to be a challenging, time-consuming and experience-dependent task to obtain these crucial information accurately. For example, a review from Nienaber et al. (2016) reports for the diameters, interoperator and intraoperator measurement variabilities numbers of $\pm$ 5 mm and $\pm$ 3 mm, respectively.

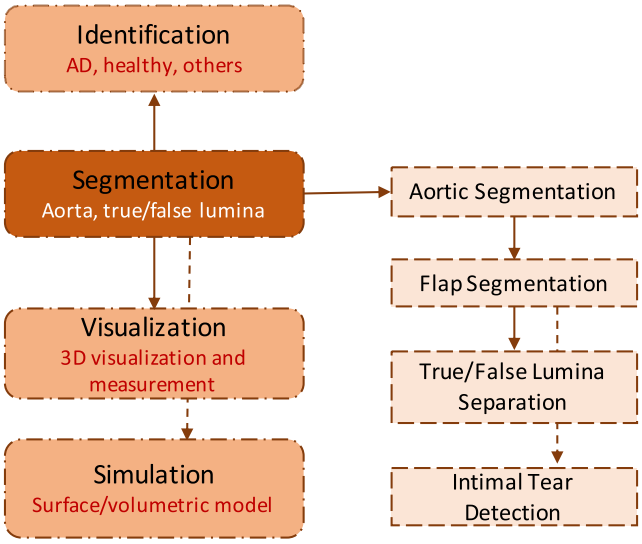

Fig. 4. AD segmentation as the core step for other AD-related analysis and applications. Solid lines indicate direct connections, e.g., from the segmentation to the visualization, while dashed lines indicate a skip of the module they go through, e.g., the segmentation can skip the visualization and go directly to the simulation.

Fig. 4 shows that the AD segmentation is the core step for other AD-specific analyses and applications such as 3D visualization of the lumina, measurement of the luminal diameters, and creation of surface or volumetric models for hemodynamic simulations (Bucurenciu et al. (2019)). For some of the computer-aided systems that identify AD in CT images automatically or semi-automatically, the aortic segmentation is usually required as the first step to create the region of interest (ROI). AD can be segmented using several successive steps: segmentation of the whole aorta, segmentation of the intimal flap, also known as dissection membrane, and the separation of true and false lumen. The intimal tear can be located on the segmented intimal flap.

Fig. 5 shows the overall components of computer-aided AD management, in which AD segmentation plays the key role. Most of the time, contrast agent is used for computed tomography (CT)

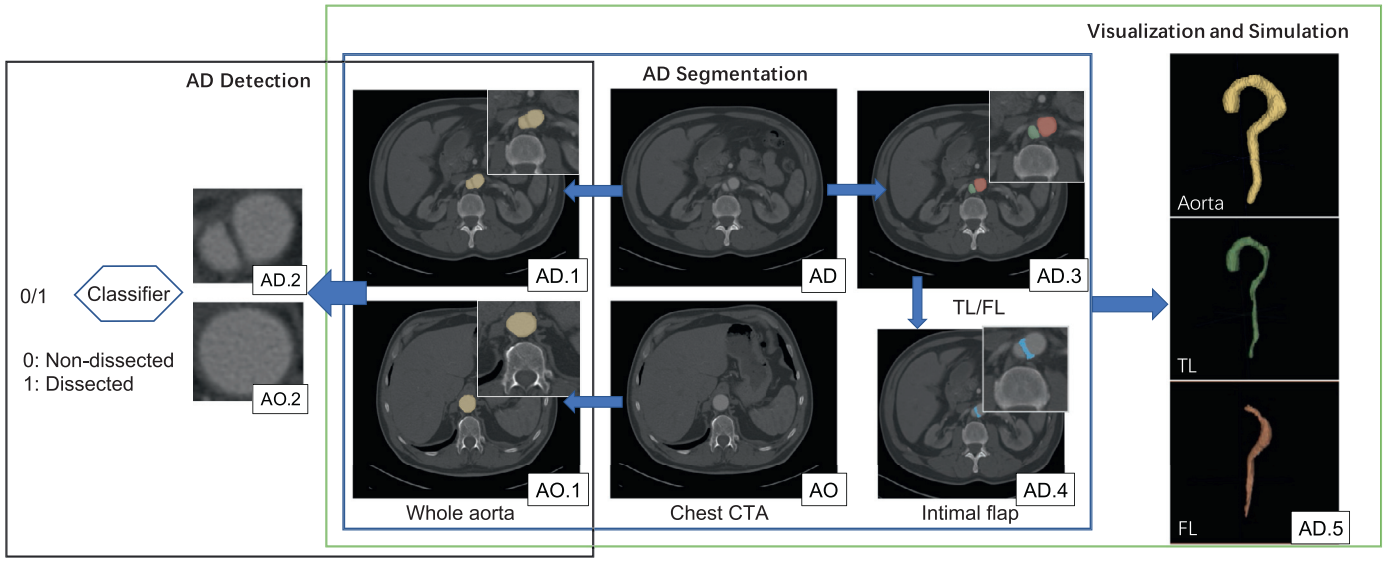

Fig. 5. Overall components of computer-aided AD management. Images labeled as *AO* show non-dissected aortas, while images labeled as *AD* show dissected aortas. As a first step, automatic aortic segmentation from CTA images (AD, AO) is performed to obtain the whole aortic region, which is the ROI. The ROI is then sent to an automatic AD diagnosis system to classify it as either a dissection (AD.1, AD.2) or a non-dissection (AO.1, AO.2). For AD treatment, the true and false lumina (AD.3), and intimal flap (AD.4) are further segmented to enable an automatic quantification of their geometric features, which helps the design and placement of patient-specific stent grafts. The geometry of the aorta, the true and false lumina can also be used for AD related research (AD.5), such as AD simulation, which can in return give insights into how an AD treatment can be improved.

AD imaging. Given a contrast-enhanced CT, the whole aorta, the true lumen (TL) and the false lumen (FL) are segmented automatically. Most of the suggested methods for segmentation are semi-automatic and rely on the prior knowledge of the morphological and anatomical characteristics of the two lumina. A limited amount of studies have instead explored fully automatic, learning-based methods for this task (Cao et al. (2019); Li et al. (2019)). Computer-aided AD detection and diagnosis is generally performed in 2D cross-sectional CT slices and usually requires the aortic region to be segmented first. Both aortic shape analysis and learning-based approaches have been investigated. The acquisition of the 3D geometry, used for computer simulations, also depends on the segmentation step. Computational fluid dynamics, for example, is a widely adopted tool for understanding the mechanisms behind the formation and the progression of an AD, which can provide further insights on AD diagnosis and treatment. Besides, automatic AD segmentation also brings the prospect of a fully automatic AD management system, where the geometric properties of an AD – luminal diameter, overall volume and location of the intimal tears – can be automatically measured. In the following sections, we provide a qualitative synthesis of the suggested algorithms for each component.

3. Computer-aided AD segmentation: A review of algorithms

While a large number of studies have focused on computer-aided segmentation of the aorta (Lesage et al. (2009)), the segmentation of dissected aortas, including true lumen, false lumen, intimal flap and outer wall, has been less intensively investigated, despite the strong clinical relevance. The unavailability of public datasets of ADs might represent a major factor for this. For the segmentation of healthy aortas, the methodologies range from established image processing techniques such as level-set (Kurugol et al. (2012); Martínez-Mera et al. (2013)), region-growing (Martínez-Mera et al. (2013); Seada et al. (2016b)) and model-based approaches (Behrens et al. (2003); Lubniewski et al. (2012); Xie et al. (2014); Seada et al. (2016)), to emerging approaches such as machine learning (Vitanovski et al. (2012)) and deep convolutional neural networks (CNNs) (Trullo et al. (2017); Noothout et al. (2018)). The segmentation of dissected aortas, even without a semantic distinction of true and false lumina, has proven to be a more challenging task than the segmentation of healthy aortas due to the presence of intimal flaps, unpredictable shape changes, and intensity attenuation in the false lumen (Morariu et al. (2014a)).

In this section, a systematic review and comparison of computer-aided AD segmentation methods is conducted, starting from very early approaches to the most recent methodologies reported in the literature.

3.1. Model-based approaches

In 2006, Kovács et al. (2006a,b) introduced a computer-aided diagnosis system that can segment the aorta, detect the intimal flap and identify true and false lumina successively and fully automatically. Utilizing the prior knowledge of the circular shape of the aorta and the Hough transform, the authors could segment the dissected aorta, regardless of the intimal flap and the inhomogeneous distribution of the contrast agent in the false lumen. The segmented aorta is further refined using an elastically deformable model (DM); the seed points for the DM can be initialized either manually or automatically on the basis of the anatomical prior information regarding the shape of the aortic arch. The proposed approach was evaluated on 21 3D CTA images of healthy aortas, dissected aortas and other pathological aortas, including aneurysms, stenoses and stent grafts. It is foreseeable that, also according to the authors' considerations, the approach fails on some cases of aortic aneurysms and stenoses, as the approach strongly relies on the prior information. It presents limitations when segmenting aortas with strong variations of the diameter length. For the validation, a ground truth segmentation was obtained manually and an average distance is used to quantify the segmentation performance of the system. Then, the intimal flap is detected within the segmented and straightened aorta by adopting the sheetness measure

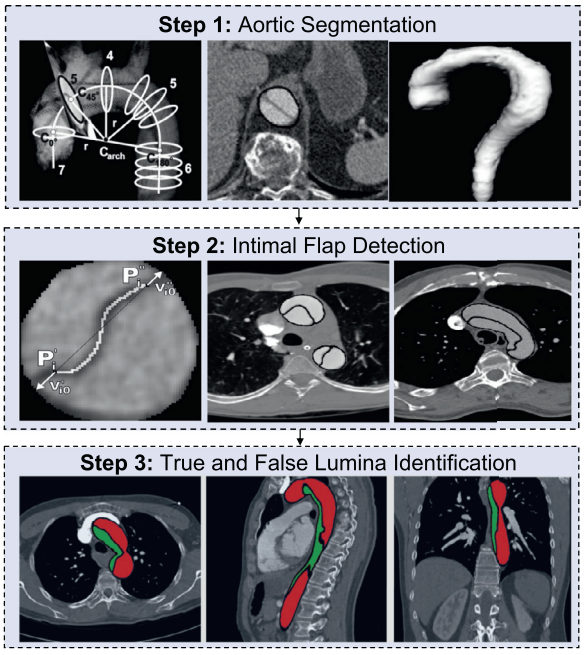

Fig. 6. Three-step approach for AD segmentation. Step 1: aortic segmentation (Kovács et al. (2006b)). Step 2: intimal flap detection (Kovács et al. (2006a)) and Step 3: true (green) and false (red) lumina identification (Kovács (2010)). (For interpretation of the references to colour in this figure legend, the reader is referred to the web version of this article.)

proposed by Descoteaux et al. (2005), and the Hessian matrix. The intimal flap detection is dependent on the aortic segmentation for the creation of a ROI, therefore it fails on aneurysmatic aortas. For the proposed design, the approach also fails on highly folded flaps where more than two aortic lumina are visible, since it relies on a specific prior model of the flap.

Finally, Kovács (2010) described in his doctoral thesis how true and false lumina can be identified and segmented following the described steps. For TBAD, true and false lumina can be distinguished on the basis of the a priori assumption that the true lumen is connected to the undissected ascending aorta. For TAAD, the cross-sectional area is used as an indicator to discriminate between the true and the false lumen, on the basis of the a priori assumption that the false lumen has a larger cross-sectional area compared to the true lumen in TAAD. These operations are performed in a multiplanar reformatted space: after the identification of the two lumina, the straightened true and false lumina are transformed back into the original coordinate system. The back-transformation process can cause errors, especially in highly curved areas such as the aortic arch.

To summarize, Kovács et al. (2006a,b) proposed a fully automatic method to segment the true and the false lumina. The authors achieved this goal with three successive steps: segmentation of the aorta, detection of the intimal flap and identification of the two lumina. Fig. 6 illustrates the process. Each step is highly dependent on the preceding steps and the model-based approach exploited, to a large extent, the a priori assumption of the morphology and properties of ADs in CTA images, which made the approach prone to failure on irregularly-shaped aortas, such as aortas with aneurysms and heavy stenoses. Another model-based approach to identify and segment true and false lumina is provided by Fetnaci et al. (2013), who proposed a modified deformable model. In particular, the authors have adapted the speed terms of the fast marching method to obtain separated lumina.

3.2. Wavelet analysis

Lee et al. (2008) introduced an approach, which combines multi-scale wavelet analysis and generative-discriminative model matching to discriminate and segment the true lumen and the false lumen. First, the complete boundary of the aorta was detected using a semi-automatic method, which was proposed by Tek et al. (2005). Second, wavelet-analysis was used to detect edges within the dissected aorta. In this step, the edges separating the true lumen from the false lumen were also detected. Third, the detected edges were refined using discriminative learning and only the lumen edge points were predicted. Fourth, generative learning was used to discriminate the true lumen and the false lumen by estimating the density distribution within the boundary of the aorta. The authors report their results on CTA images of AD, but no information is given in regard to the performances of thrombosed false lumina, multiple false lumina, or other less common shapes.

3.3. Deep learning

While deep CNNs are playing an increasingly important role and achieving state-of-the-art results on many medical image segmentation tasks (Ronneberger et al. (2015); Milletari et al. (2016); Li et al. (2018)), the application of CNNs in the segmentation of ADs has been underinvestigated. Li et al. (2019) used two 2D cascaded convolutional networks to extract the contours of both the aorta and its true lumen. Different from traditional binary masks, only the lumen contours are manually annotated with a fixed number of points. To our knowledge, Li et al. (2019) is the first group to tackle the problem of AD segmentation using deep learning. Cao et al. (2019) designed a 3D U-Net that can segment true lumen and false lumen simultaneously in a unified network, based on a large collection of CTA datasets, and manually annotated in a voxel-wise manner. True lumen, false lumen, and the overall aortic lumen in CTA images have been manually segmented, which is a time-consuming, labor-intensive and expensive task. We summarize the difference and similarity between the two deep learning-based approaches from the perspective of AD annotation, segmentation network and their results.

AD Annotation Cao et al. (2019) formulated AD segmentation by extracting the whole region of the lumina, which is common in the image segmentation field, while Li et al. (2019) thought of AD segmentation as the extraction of only the luminal contours, and the whole luminal region can be obtained with simple post-processing operations. The different formulation of the problem has lead to different AD annotation strategies from the two groups. Cao et al. (2019) constructed a dataset containing 276 CTA images from patients with TBADs. For each CTA image, experts created manually the mask for the whole aortic lumen, true lumen and false lumen separately, using an open-source software (3D Slicer, https://www.slicer.org/). Each image was annotated in a slice-wise manner and it can be imagined that this constitutes a labor-intensive annotation process. On the contrary, Li et al. (2019) collected 45 contrast-enhanced CT images (both type-A and type-B AD are included, with 4963 slices altogether) and annotated the contour (edges) of the whole aorta and true lumen separately, each using a fixed number of points (38). They also used an open-source software (ITK-SNAP, www.itksnap.org) for annotation. Both studies claim that the annotation was performed by experts, whereas currently none of them has released a detailed description of the annotation protocol to ensure reproducibility. In the study of Cao et al. (2019), it is unclear how they define the aortic wall and the intimal flap when annotating both the true lumen and the false lumen within the whole aortic region. It should be noted that the boundary of true and false lumina is sometimes very ambiguous and both the aortic wall and the intimal flap are

Table 1
List of studies on aortic dissection segmentation (*core papers*). (Auto: Fully automatic, Avg: Average, CNN: Convolutional neural network, CT: Computed tomography, CTA: Computed tomography angiography, Dist: Distance, DSC: Dice similarity score, FL: False lumen, H.Dist: Hausdorff distance, HM: Hessian matrix, HT: Hough transform, LS: Level set, Sen: Sensitivity, Spe: Specificity, TL: True lumen, WA: Wavelet analysis)

Publication	Method	Auto	Dataset	Metric	Comments	Annotation	Availability
Kovács et al. (2006a)	HM	✓	CTA	Avg Dist	Intimal flap	-	-
Kovács et al. (2006b)	HT	✓	CTA	Avg Dist	Whole aorta	-	-
Lee et al. (2008)	WA	×	-	Sen, Spe	Type A and B	Contour	×
Kovács (2010)	Priori	✓	CTA	Avg Dist, H.Dist, DSC	TL, FL	-	-
Fetnaci et al. (2013)	LS, FM	×	CT	-	TL, FL	-	-
Cao et al. (2019)	3D U-Net	✓	CTA	DSC	Type B	Region	×
Li et al. (2019)	2D CNN	✓	CTA	DSC	Type A and B	Contour	-

very thin structures in CTA images, which is a detail that leads to subjectivity when performing manual annotation.

Segmentation Network Li et al. (2019) used two independent 2D cascaded CNNs to extract the contours of the whole aortic lumen and the true lumen separately. The false lumen contour can be obtained through an easy conversion from the contours of the whole aortic lumen and the true lumen. Instead, Cao et al. (2019) used two 3D segmentation networks: the first network was used to segment the whole aorta, while the second was used to segment true lumen and false lumen simultaneously. Restricted by computational resources, both of the two studies reported a down-sampled CT image as the input of the network. Li et al. (2019) down-sampled the slices from 512 × 512 to 144 × 144 and Cao et al. (2019) down-sampled the volume to 128 × 128 × 256 voxels, but did not state the original volume size. Memory limitation represents a common challenge in medical image segmentation using deep learning as medical images usually come with high in-plane resolution of 512 × 512 voxels. Down-sampling can severely deteriorate the image content and cause a loss of image quality for the CT data as well as the ground truth annotations, leading to poorer predictions of the trained neural networks. Some of the side-effects of down-sampling are briefly discussed by Cao et al. (2019). Data augmentation during training was adopted in both studies.

Results The two studies used the DSC as the comparison metric. The average DSC for Li et al. (2019) was 0.989 for the whole aorta and 0.925 for the true lumen on a five-fold cross-validation of 45 CT volumes. No test set and test results are provided. Cao et al. (2019) used 246 CTA scans for training and 30 for testing. The testing results were 0.93, 0.93, and 0.91 for the whole aorta, the true lumen and the false lumen, respectively. The authors also reported a three-fold average validation DSC of 0.93, 0.92 and 0.91 for 30 randomly selected CTA scans from the training set. The reported training time is 71 h (21 h for the *adventitia network* and 50 h for the *intima network*) on a GTX 1080 Ti GPU for Li et al. (2019), while Cao et al. (2019) did not report this information. The latter reported an average inference time of 31.06 s including down-sampling (6.68 s), inference (6.28 s) and post-processing (18.1 s). However, it is difficult to directly compare the performance of the two approaches since different, non-public datasets have been used in each study. The output of the proposed segmentation network of Li et al. (2019) consists of 2D contour points of a slice. The 3D lumen mesh model of the whole aortic lumen and the true lumen can be obtained by triangulating the contour points of the adjacent slices. For the network of Cao et al. (2019), the output is directly the 3D volume of the whole aorta, and the true and false lumina.

3.4. Summary

To summarize, in this section we reviewed the reported approaches for AD segmentation, more specifically, the segmentation of true lumen and false lumen. To our knowledge, so far, the investigated papers above represent all existent studies that target specifically at the segmentation of the two lumina. The approaches can roughly be divided into two categories, i.e., (i) classical image processing methods and (ii) deep learning-based approaches. For the first category, model-based approaches and the Hessian matrix are most widely used. The approaches reported in this category of publications are usually a combination of multiple classical image processing methods and consist of multiple steps, making them less straightforward and prone to failure after each step.

On the contrary, from a high-level perspective, the two deep learning-based approaches are relatively more straightforward, i.e., take as input the contrast-enhanced CT images and provide as output the segmentation of the two lumina. However, the described deep learning-based approaches require large, manually annotated datasets for supervised training, which are generally difficult and expensive to obtain. It is clear that initial research used classical image segmentation methods, while more recent research opts for deep learning approaches, due to their successful applications in different segmentation tasks (Ronneberger et al. (2015)). As analyzed above, both the contour-based and the mask-based learning have advantages and disadvantages and it is natural to come to the assumption that future deep learning-based segmentation methods for ADs should consider both, the contour and the mask, in the learning process of the network, to improve its performance. Publications associated with AD segmentation are summarized in Table 1.

It is also worth mentioning that the reviewed deep learning approaches do not handle less common variants of AD such as multichannel AD, where more than two lumina are present, or post-operative images where a metal stent graft is visible or an aneurysm coexists with the dissection. The segmentation performance for thrombosed false lumina is also not stated. Cao et al. (2019) briefly stated that prediction errors mostly arise from uncommon dissection cases – dissections with an aneurysm, tortuous descending aortas and anatomic abnormalities. In addition, Li et al. (2019) also pointed out that their deep learning model produces inaccurate results also in areas where the true and false lumina appear to be similar with respect to shape and voxel intensity. The voxel intensity, and therefore the distribution of the contrast agent in a dissected aorta is often uneven due to the presence of intimal tears and FL thrombosis. This can potentially affect the performance of deep learning models for segmentation. We will further discuss this issue in Section 5.2 of this review.

Both Cao et al. (2019) and Li et al. (2019) speculate that the inclusion of more uncommon cases in the training set could lead to more robust models. Therefore, the training and evaluation datasets for AD segmentation should be carefully designed and include a balanced number of cases for each situation.

Overall, both deep learning-based methods and the more *classical* segmentation methods do not provide a solution which correctly handles also the uncommon AD cases. The classical methods

Table 2
List of published studies related to computer-aided diagnosis, treatment, visualization and simulation of AD (*additional papers*): CFD: Computational fluid dynamics; CNN: Convolutional neural network; CT: Computed tomography; CTA: Computed tomography angiography; FSI: Fluid–structure interaction; GFSC: Greedy fine structure completion; GVF: Gradient vector flow; MDCT: Multi-detector CT; MRI: Magnetic resonance imaging.

Publication	Methodology	Dataset	Comments
		Outer wall and flap segmentation	
Krissian et al. (2014)	Level-set methods	MDCT	Intimal flap segmentation
Lohou et al. (2014)	Morphological operators	CTA	Intimal flap segmentation
Morariu et al. (2014a)	Polar-based method	CTA	Dissected aorta segmentation
Morariu et al. (2014b)	Graph-based method	CTA	Dissected aorta segmentation
Morariu et al. (2015)	Spectral phase analysis	CTA	Intimal flap segmentationn
Morariu et al. (2016a)	GFSC	CTA	Intimal flap segmentation
Morariu et al. (2016)	Phase congruency	CTA	Intimal flap segmentation
Morariu et al. (2016c)	Template filter and fuzzy c-means	CTA	Intimal flap segmentation
Xiaojie et al. (2016)	Spatial continuity prior model	CTA	Intimal flap segmentation
Eigen et al. (2018)	Active-contour model	CTA	Dissected aorta inner and outer wall extraction
		Detection	
Lohou and Miguel (2011)	3D hole filling	Enhanced CT	Intimal tear detection
Gayhart and Arisawa (2013)	Fast circle detection	Enhanced CT	AD detection
Dehghan et al. (2017)	Hessian matrix	Enhanced CT	AD detection
Duan et al. (2018)	GVF snake model	CT	AD detection
Harris et al. (2019)	2D CNN	Enhanced CT	AD detection
Xu et al. (2019)	CNN	CTA	AD detection (Type A)
		Simulation	
Bazilevs et al. (2009)	FSI	CT	Fontan configuration
Bazilevs et al. (2010)	FSI, CFD	MRI, CT	Review
Crosetto et al. (2011)	FSI	MRI	Simulation of aorta
Chen et al. (2013)	CFD	CTA	Blood flow in AD
Alimohammadi et al. (2014)	CFD	CTA	Virtual device deployment in AD
Menichini et al. (2018)	CFD	CTA	Thrombus formation in AD
Bucurenciu et al. (2019)	CFD	CTA	Simulation of chronic TBAD
Qiao et al. (2019)	FSI	CTA	Simulation of AD
Bäumler et al. (2020)	FSI	CTA	Simulation of AD
		Visualization	
de Hoon et al. (2014)	CFD, flow visualization	MRI	Simulation-enhanced 4D flow MRI
Mistelbauer et al. (2016)	Ad hoc, 2D plots	CTA	Visual risk assessment
Qi et al. (2016)	Virtual intravascular endoscopy	CTA	Intimal tear visualization
Burris et al. (2017)	Vascular deformation mapping	CTA	Intra-patient mapping and visualization

generally rely on an a priori assumption of the dissection morphology, which cannot cover all the variations of the uncommon cases. Each subcategory would therefore require its own ad hoc solution. However, this would considerably affect the complexity of a comprehensive computer-aided segmentation system. An alternative is given by deep learning models, which appear to move the complexity to a level of data collection and annotation. Additionally, a focus on robust and automatic vessel tree segmentation for AD datasets appears to be still missing.

4. Additional studies

According to our investigation above, only a limited number of studies focus specifically on the segmentation of true and false lumina, which is a complex task. In this section, we review some studies that do not target directly at the segmentation of the two lumina but are highly relevant to AD treatment and diagnosis in clinical routines. Publications associated with computer-aided diagnosis and treatment of ADs are summarized in Table 2. At the end of each subsection, we discuss how the reviewed papers addressed the problem of irregular AD cases such as multichannel AD, aneurysm, thrombosis and non-uniform contrast distribution, if relevant information is provided in the papers.

4.1. Intimal flap detection and segmentation

The segmentation of the intimal flap from dissected aortas is considered to be a challenging task due to its great morphological variability. Intimal flap segmentation is also considered to be a prerequisite step for other tasks such as intimal tear detection and segmentation of true and false lumina. For most of the investigated studies regarding the intimal flap segmentation, the first step is to segment the entire dissected aorta, and then the intimal flap is segmented within the ROI. Morariu et al. (2014b) first introduced a graph-based approach for the segmentation of dissected aortas from CTA images. In subsequent studies, several approaches were proposed to extract the flap from the segmented aorta. Morariu et al. (2015) exploited spectral phase information to deal with the high variability of luminance and contrast, and with the presence of artifacts, which is common in CTA images. Morariu et al. (2016a) proposed greedy fine structure completion, a framework to detect fine structures in medical images, and successfully applied the framework in the segmentation of the intimal flap in CTA images, where the surrounding environment (e.g., contrast) is inhomogeneous. The two lumina (true and false) can then be separated using the segmented flap. Morariu et al. (2016) introduced 3D phase congruency for flap detection and obtained an average error of 1.1 mm against ground truth. Morariu et al. (2016c) introduced a parameter-free approach based on template filter and fuzzy c-means clustering to detect arbitrarily oriented ridge-shaped components in CTA images, yielding a sub-millimeter average error against ground truth.

Krissian et al. (2014) described a two-stage approach to delineate the intimal flap semi-automatically from multi-detector CT. In the first stage, the centerline of the aorta including the main branches is obtained semi-automatically. In the second stage, the outer wall of the aorta including the main branches is segmented automatically under a level-set framework that uses region growing for an initial rough segmentation. Then, the intimal flap is segmented as a 3D polygonal mesh from the segmented aorta. The signed distance between the triangular mesh of the intimal flap

obtained by the approach and manual delineation is used to quantify the performance, yielding a mean absolute distance value of no more than half a voxel. The limitation of the proposed method lies in four aspects. First, it can lead to inevitable false positive detection on healthy aortas due to the presence of varying intensities in the reconstructed aorta. Second, it focused only on the segmentation of outer wall and intimal flap without identifying true and false lumina. The third limitation is that only five real AD cases were involved in the evaluation of the approach. Fourth, the performance of the methods can be affected by a number of parameters that require manual tuning, which can be time-consuming in specific cases. Additionally, thrombi cases are considered out of scope in their work. In Lohou et al. (2014), simple morphological operators were adopted to segment the intimal flap from CTA images after segmenting true and false lumina by using the methods described in Fetnaci et al. (2013). Demos et al. (1986) presents a case report to detect the intimal flap in non-enhanced CT. Xiaojie et al. (2016) suggest a spatial continuity prior model to segment the intimal flap. The authors first segment the overall aorta using gradient vector flow snakes, then apply the suggested model for the segmentation of the flap. The approach has been only tested on descending aortas and no information is provided with regard to inhomogeneous contrast, false lumen thrombosis, or multiple false lumina.

Discussion According to the literature, intimal flap segmentation generally requires different steps and the results are therefore sensitive to the accuracy of each single step, especially for uncommon AD cases. In the approach proposed by Krissian et al. (2014), the segmentation step is known to fail on thrombosed AD cases. In the serial studies of Morariu et al. (2015, 2016a, 2016b, 2016c), the first step – segmentation of the AD – can be affected by the tortuous aortic morphology caused by severe pathologies or previous surgeries, which can lead to an erroneous segmentation when using the traditional Hough transform and, therefore, affect the following steps. To deal with this problem, the authors introduced a graph-based approach to optimally localize the cross-section in a multi-planar reformation. A 2D deformation is further applied to the localized cross-sections to fit the irregular shape of the aorta. Another common issue in segmentation is caused by unequal contrast distribution in CTA images. Traditional intensity-based segmentation approaches tend to fail in situations where the contrast varies greatly among datasets or among slices in the same dataset. To address the problem, the authors proposed the use of phase information in the frequency domain (Morariu et al. (2015, 2016)), which is robust to contrast variability. The contrast-invariant approach allows the segmentation of fine structures, such as the intimal flap, in CTA images even in the presence of image artifacts. Morariu et al. (2016a) addressed the problem of the high morphological variability of the intimal flap in segmentation. The high variability of the intimal flap morphology can lead to failure of segmentation approaches that are based on predefined shape priors.

The four studies of Morariu et al. (2015, 2016a, 2016b, 2016c) use annotated CTA datasets of TAAD in their evaluation phase instead of the development phase, no data-driven, learning-based approach is found to be reported for intimal flap segmentation so far.

4.2. AD Detection and identification

Aortic dissection detection is to distinguish between healthy aorta and dissected aorta in CTA or CT images. The goal of computer-aided AD detection is to ease the diagnostic process for radiologists. Even if AD can be easily recognized in CT or CTA images, the diagnosis of AD is usually performed by clinicians in a slice-wise manner, which is very time-consuming and liable to misdiagnosis especially when dealing with high volume medical images. In Gayhart and Arisawa (2013), the discrimination between dissected and healthy aortas is based on the shape of detected edges. First, the aorta is segmented from contrast-enhanced CT images on the basis of the Hounsfield unit range in the lumen and its anatomical shape. Second, a fast circle detection method (Rad et al. (2003)) is adopted to detect pixels belonging to a circle-like edge in a 2D slice. The slice is considered healthy if the number of such pixels reached a predefined threshold, otherwise the slice is considered to be dissected. The approach was evaluated on 479 slices from five cases and obtained a sensitivity of 0.8218 and a specificity of 0.9907. Given that the aortic segmentation and the dissection recognition are based on the pre-observation about the pixel intensity within the lumen and the dissection shape (i.e., the healthy aorta is circle shaped), it is understandable that it fails on less common cases, which contradict the pre-observations. Dehghan et al. (2017) identifies ADs on the basis of the abnormal shape of the dissected aorta and the existence of intimal flaps. Similar to Gayhart and Arisawa (2013), the aorta is first segmented using an atlas-based method to obtain the ROI in the contrast-enhanced CT images. Then a multi-scale flap enhancement filter based on a Hessian matrix is applied to each slice to obtain the ridge-like intimal flap. The separation of the true lumen from the false lumen by the detected flap is used as an indicator of the existence of a dissection on the slice. The separation of the two lumina can be identified by the number of connected components. If, in a cross section, the flap does not extend from one side of the aorta to the other (i.e., the two lumina are not completely separated) or the false lumen is thrombosed, the segmented cross-sectional aorta depicts low circularity so that a dissected aorta can be identified using a circularity measure and threshold. In this sense, false lumen thrombosis is beneficial for detection. However, considering the huge dissection variability, it can be envisaged that using a fixed threshold cannot work optimally for all dissection cases. After performing slice-wise detection, the patient-level category is determined by the number of positive slices in a 10-slice window and a pre-defined threshold. The atlas-based aorta segmentation can fail due to the existence of a severe aneurysm, which deforms the aortic shape and can further lead to false positive AD detection. In this work, true and false lumina can be separated and segmented by the detected intimal flap but no information is provided to further differentiate the two lumina.

In Harris et al. (2019), a 2D CNN is trained to classify non-AD aortas, AD and aortic rupture from contrast-enhanced chest CT images in axial view. The dissection is detected on the entire cross-sectional slice instead of a ROI (segmented aorta), which is different from Gayhart and Arisawa (2013), and Dehghan et al. (2017). 778 post-contrast CT studies (279 non-AD, 471 AD, 28 aortic rupture) were collected for training and 118 (50 non AD, 50 AD and 18 aortic rupture) for testing, yielding a sensitivity and specificity of 0.878 and 0.960 for ADs, respectively. The category of an entire CT study containing multiple axial slices is determined by the number of positive slices (slices with AD) and a pre-defined threshold. The automated diagnostic process is integrated into a teleradiology workflow in a hospital, which reduces the time required for radiologists to review the scans. Xu et al. (2019) trained two ResNet (He et al. (2015)) to identify ADs in CTA images (TAAD). First, Mask R-CNN (He et al. (2017)) was used to segment the aorta to obtain the ROI. Then a Canny edge detector was applied to detect edges on the segmented aorta. The detected edges were used to train the 2D ResNet classifier. By considering the huge morphological differences between the aortic arch and the remaining aorta, the authors trained two separate networks to detect a dissection in the two aortic regions.

Discussion Gayhart and Arisawa (2013) distinguish between healthy and dissected aortas using the assumption that healthy aortas present circular cross sections. Nonetheless, this criterion is

not robust to the shape variability of the dissection. For example, when a true lumen is obstructed by the false lumen in a cross-sectional slice and the true lumen occupies a small portion of the overall lumen, the aorta can still be circular and therefore be erroneously classified as normal. Besides, the detection of ADs requires the aortic lumen to be segmented first. The aorta is segmented using a pre-defined threshold, which can easily lead to an over- or under-segmentation as the contrast distribution in the aortic lumen can be uneven. The study reported a high specificity but a relatively low sensitivity in the AD detection, which means that the approach fails to recognize some dissection morphologies, as also discussed in the previous example. Together with the measure of shape abnormality, Dehghan et al. (2017) incorporated an additional indicator – the presence of an intimal flap. The use of this additional criterion increases the robustness of detection algorithms and compensates for shape irregularities caused by aortic pathologies other than dissection, such as the aneurysm. However, *severe* aneurysms can still lead to false positive detection as it can cause the failure of the aortic segmentation in the first step and the segmented aorta can depict high irregularity so that it is classified as a dissection according to the shape abnormality measure. The work excludes post-operative CT slices where a stent graft is present for aortic detection.

Data-driven approaches are also popular in this category. Harris et al. (2019) analysed the influence of aneurysms in false positive predictions of the proposed deep learning model. The study shows that the deep learning model is significantly more likely to recognize aneurysm cases as positive dissection than as non-dissection. Morphological changes (e.g., degeneration) of the aorta caused by, e.g., aging is another factor the study revealed that can cause a false positive detection. Besides the inclusion of more data into the training set, the authors mentioned that retraining the deep learning model with only the falsely classified cases can help to reduce the false positive and false negative predictions. In Xu et al. (2019), no information is provided about the limitation factors related to uncommon dissection morphology or uneven contrast distribution.

To summarize, most of the existent AD detection approaches require that the aorta is segmented first to create the ROI with the exception of the study by Harris et al. (2019), which detected the AD on the entire cross-sectional slice. The quality of the aortic segmentation can affect the detection accuracy. Earlier approaches tend to adopt classical image processing algorithms to obtain the ROI and to identify AD, while most recent approaches, such as the one by Xu et al. (2019), prefer to use CNNs for both segmentation and classification. In addition, all the reviewed papers in this category present approaches to detect a dissection in contrast-enhanced CT images. Harris et al. (2019) mentioned that if the CTs are not enhanced by a contrast agent, it is prone to a false negative detection. All the papers detect ADs on 2D slices, whereas Gayhart and Arisawa (2013), Harris et al. (2019) and Xu et al. (2019) further inferred the slice-wise predictions to a patient level (i.e., the whole 3D volume).

For AD detection, both the shape analysis-based papers and the deep learning-based papers, such as the one by Harris et al. (2019), have mentioned that dissection irregularities such as aneurysm and contrast inhomogeneity can have negative effects on their detection algorithms but the issue has not yet been solved by their methods. Much like the AD segmentation, as discussed in Section 3.4, for deep learning-based detection, the common recommendation is to include more data in the training set or, alternatively, to retrain the network with the falsely classified samples. For shape analysis-based detection, it appears unlikely that a single approach can handle all dissection variabilities. To achieve high detection accuracy, it is recommended to develop different approaches for each different morphological type.

4.3. Detection of intimal tears

The placement of a stent graft during an AD surgery is determined on the basis of the location of the intimal tear. Usually, the tear is localized on CTA images by radiologists in a slice-wise manner using intensity variations, which is time-consuming and experience-dependent. Lohou and Miguel (2011) proposed to detect the intimal tear on the manually segmented intimal flap using a 3D hole filling algorithm documented by Aktouf et al. (2002). The authors do not explicitly provide information about the performance on less common cases of ADs, such as multiple or thrombosed false lumina. The work only focuses on the detection of the intimal tears on already segmented images. For the reported cases, the segmentation was performed manually.

4.4. AD Visualization and automatic analysis

After an AD has been segmented, it enables several possibilities for an automatic analysis. Very basic features of the aorta include, e.g., the diameter, which is on average between 3 and 4 cm (Mao et al. (2008); Paruchuri et al. (2015)), and the length of the aorta, which is between 30 and 40 cm (Dotter et al. (1950)). Features that are more sophisticated are the location and angle of the branching vessels of the aorta (Demertzis et al. (2010)), like the renal (Lauder et al. (2018)) and iliac arteries (Szpinda et al. (2012)). To ease the analysis of these measurements, Mistelbauer et al. (2016) suggested *aortic dissection maps*, a comprehensive scheme to visualize the extension of the disease and the outcome of past interventions and the risk of related adverse events. Burris et al. (2017) introduced a vascular deformation mapping method to register the segmentations of follow-up CTA images and to obtain a visualization of the aortic growth. Note that the authors do not provide information about the mapping performances for the different types of AD. Qi et al. (2016) evaluated the utilization of virtual intravascular endoscopy for a more accurate understanding of the location and shape of intimal tears, which can be otherwise challenging using raw CTA images. The segmentation also allows the monitoring of a dissection development over time for a patient subject to regular follow-up screenings, including the development of a thrombus in the false lumen (FL) (Olabarriaga et al. (2005)), and the helical pattern along and around the true lumen (TL) (see, e.g., Gültekin et al. (2019)). Fig. 7 presents a segmented TL (green) and FL (red) from a CTA scan of a patient with an AD, and shows how the FL wrapped around the TL. Besides, synthetic models of aortas and ADs (also over time) can be used as data augmentation (Wong et al. (2016); Shorten and Khoshgoftaar (2019)) to feed deep neuronal networks, where, in general, a large amount of labeled training datasets is otherwise needed. Finally, de Hoon et al. (2014) suggested an interesting approach to enhance the blood flow visualization in 4D MRI images. To overcome the limitations of the spatio-temporal resolution in 4D MRI, the authors suggested a flow visualization method which merges the information from the 4D MRI with a hybrid simulation model on the basis of computational fluid dynamics (CFD).

4.5. Vascular simulations of ADs

Finally, AD segmentations can be used in precise and patient-specific vascular simulations (Bucurenciu et al. (2019)). However, constructing a 3D patient-specific numerical model to perform vascular simulations requires a discretized, high-quality geometry of the computational domain. Therein, the created mesh has to describe a 3D geometry accurately enough to study how the hemodynamics is affected by the vessel wall geometry and the chosen

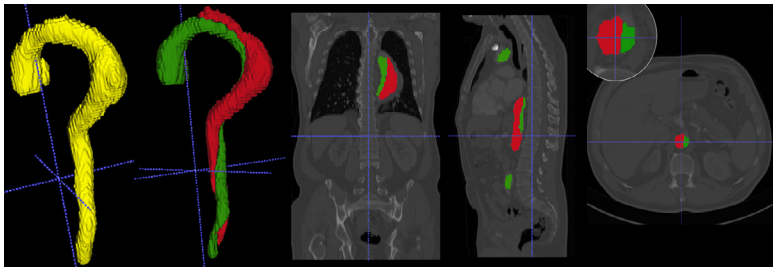

Fig. 7. Helical pattern of the false lumen (red) along and around the true lumen (green) of a segmented CTA scan of a patient suffering from an AD. From left to right: whole aorta (yellow), true/false lumen in 3D, true/false lumen in coronal, sagittal and axial views. (For interpretation of the references to colour in this figure legend, the reader is referred to the web version of this article.)

boundary conditions, but coarse enough to limit the computational effort (Bazilevs et al. (2010)). The solution of complex 3D and time-dependent boundary-value problems is typically approximated using numerical methods like the finite volume or the finite element method. The former is typically used in the computational modeling of fluids, whereas the latter dominates the field of solid mechanics. The numerical approach on modeling the interaction of the fluid and solid fields is known as fluid–structure interaction (FSI). Within FSI, the balance of stresses, velocities and displacements at the interface of the fluid and solid domains dominates the behavior of the coupled system in the cardiovascular setting. The interface description may be given implicitly or explicitly, depending on the method of choice. Yet, an explicit description of the fluid and solid subdomains enables the use of off-the-shelf computational tools.

Additionally, in the modeling of the cardiovascular system, the thickness of the vessel and other surrounding tissues with a load-bearing effect influences highly the simulation outcome (Crosetto et al. (2011); Bäumler et al. (2020)), but obtaining a reliable patient-specific wall thickness is significantly harder than obtaining the lumen domain due to the lack of contrast to the background.

Different approaches to reconstruct the blood vessel thickness are shown in Bazilevs et al. (2009) and Ryu et al. (2009). After the wall thickness distribution is given, a volume mesh of the entire blood vessel has to be generated, which includes the vessel wall, the vessel interior, and a smooth interface between them. Furthermore, specific mesh requirements, like the generation of fluid boundary layers for accurate numerical prediction and increased stability, must be defined individually. All elements of a mesh used for numerical simulations have to meet geometric criteria on the basis of the corner angles and aspect ratios of the mesh elements. In addition, it is not permitted that elements overlap and that hanging nodes or double elements exist. These requirements are an essential component of a successful finite element or finite volume analysis. When generating a finite element mesh, this is usually started from a coarse mesh. In the course of the computation, an adaptive mesh refinement technique can be used to adapt the accuracy of a solution within a certain geometrical region when required. Yet, the geometric description, and therefore the segmentation, of the physiological domain has to be sufficiently accurate, otherwise a non-negligible error will be propagated during geometry simplification and refinement. In general, the finite element method is not restricted to certain element types, but the most widely used element types in the 3D space are hexahedral and tetrahedral elements. When creating a mesh, the construction of smooth and flat in- and outlet surfaces of the domain to impose boundary conditions accurately is another crucial aspect. Subsequently, a well generated volume mesh, created from MRI or CT images, can be imported into a finite element or finite volume software to solve the numerical model.

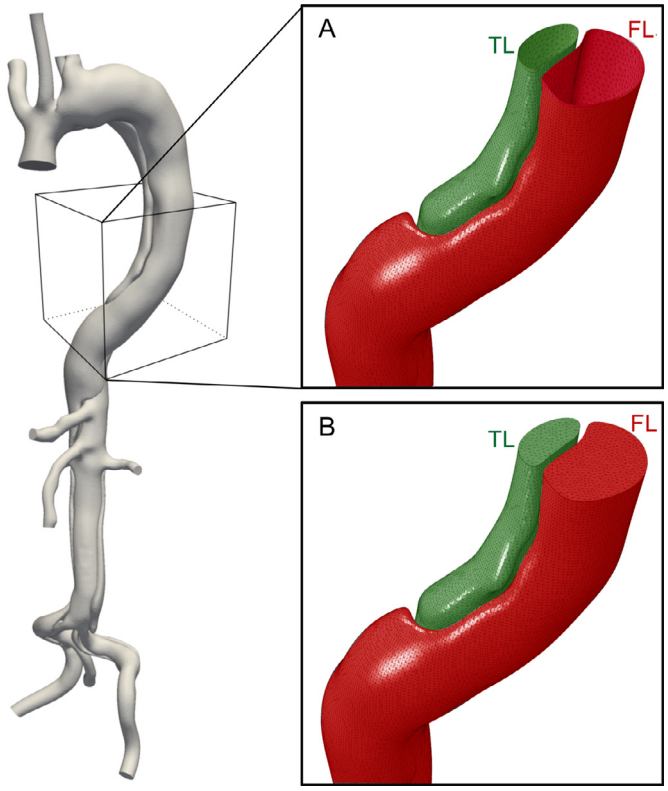

Fig. 8. Left: patient-specific mesh of a dissected aorta. Right: A) a section of the aorta as surface mesh for, e.g., 3D printing and augmented and virtual reality applications; B) a section of the aorta as volumetric model to be used as input for, e.g., a CFD simulation. Meshes processed using Abaqus FEA (http://www.simulia.com/, Dassault Systèmes Simulia Corp.) and Meshmixer (http://www.meshmixer.com/, Autodesk Inc.) (Bäumler et al. (2020)).

Fig. 8 (A) shows the section of a surface model of the aorta. Specific examples of applications for surface models are 3D printing and augmented and virtual reality applications (Ho et al. (2017); Egger et al. (2020)). Fig. 8 (B) shows the section of a corresponding volumetric model, which can be used as input for a CFD simulation. CFD simulations, for example, are commonly used to perform patient-specific blood flow simulations in AD by applying the finite volume method (Chen et al. (2013); Alimohammadi et al. (2014); Menichini et al. (2018)). In addition, the volumetric mesh can be used as input for the discretization of the aortic wall in FSI (Qiao et al. (2019)).

5. Conclusion and discussion

In this review, we presented a comprehensive summary of approaches for computer-aided segmentation of ADs (the whole aorta, true and false lumina). In doing so, the advantages and disadvantages of these approaches were analyzed and compared. Besides the literature targeted at the segmentation of ADs, we also reviewed studies that do not focus directly on the segmentation of the true and false lumina but are related to computer-aided diagnosis and treatment of the disease such as the detection of intimal tear, segmentation of intimal flap and AD recognition. One of the interesting findings is that, different from the segmentation of other organs such as liver, heart chambers, and some tumors where deep learning-based approaches are prevalent, only two research groups adopted deep learning networks as the backbone for AD segmentation. This could be attributed to the fact that large, expert annotated datasets of a rare disease are more difficult to construct than other medical datasets.

5.1. Current state

Most existing approaches are model-based and usually combine classical image processing theories such as level-set and Hough transform. These approaches rely, to a large extent, on the a priori observation of the morphology and properties of ADs in CTA images and cannot work well on irregularly-shaped aortas caused by aneurysms or stenoses. In other words, these types of approaches cannot generalize well. Besides, these approaches usually involve multiple steps to achieve the segmentation of true and false lumina, which makes them less straightforward and stable. The advantage is that they do not require large AD datasets with expert annotation for development since they are based on the a priori knowledge of ADs (e.g., morphology, intensity and other observed properties). However, they usually need expert annotated AD cases in the evaluation phase so that they can compare the results generated automatically or semi-automatically by their approaches with the ground truth. On the other hand, from a workflow perspective, deep learning-based approaches can be more straightforward and usually require only a single step to produce the segmentation of true and false lumina. However, their development is hindered by the lack of large, annotated and publicly available AD datasets, which are difficult to obtain. The generalization performance of deep learning-based approaches is determined largely by the datasets, which are needed both in the development phase and in the evaluation phase. To our best knowledge, so far, not a single clinically applicable computer-aided AD segmentation system has been reported, which means that the field is still worth to investigate in more detail.

5.2. Future directions

The deep learning studies, as presented in Section 3.3, mentioned that a larger dataset containing AD cases with more morphologies, especially the less common dissection morphologies, will be considered in their future works. Li et al. (2019) pointed out that, for some AD cases, the contour of the true lumen is not closed and may present a more complex shape, which is not included in the training set or the number of similar cases is relatively small. It is foreseeable that the segmentation networks will not provide a correct prediction for these cases, which sets a limitation for the current approaches. To cope with the existing limitations, it is also possible to correlate deep learning-based AD segmentation approaches with classical AD segmentation methods, mainly model based, which also fail on uncommon dissection morphologies. This problem should be addressed properly in future AD segmentation research. Cao et al. (2019) moved a step further to consider an automatic measurement of anatomical AD features on the basis of the automatic AD segmentation, which is a good step towards building a clinically applicable AD segmentation and computer-aided surgery system. Methodologically, it is also worth comparing the segmentation performance between contour-supervised learning (Li et al. (2019)) and mask-supervised learning (Cao et al. (2019)) in future work, trained with ground truth masks, a segmentation network will basically learn the gray value distribution in the true lumen, the false lumen and the background during training. Therefore, the network can segment and distinguish between the two lumina and infer using the difference of the learned distributions.

In Fig. 9 (top) we can see that the contrast agent is usually distributed unevenly in the aortic lumen and especially in the false lumen, while the true lumen continues to present an even distribution of the contrast agent. It will be easy for the network to

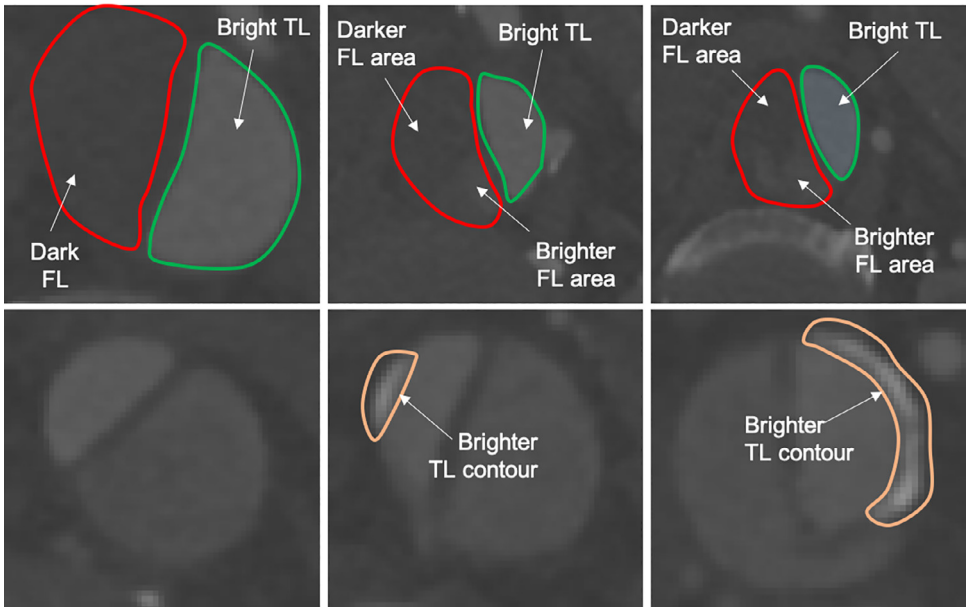

Fig. 9. The intra-class heterogeneity of the luminal region (top) and the luminal boundary (bottom).

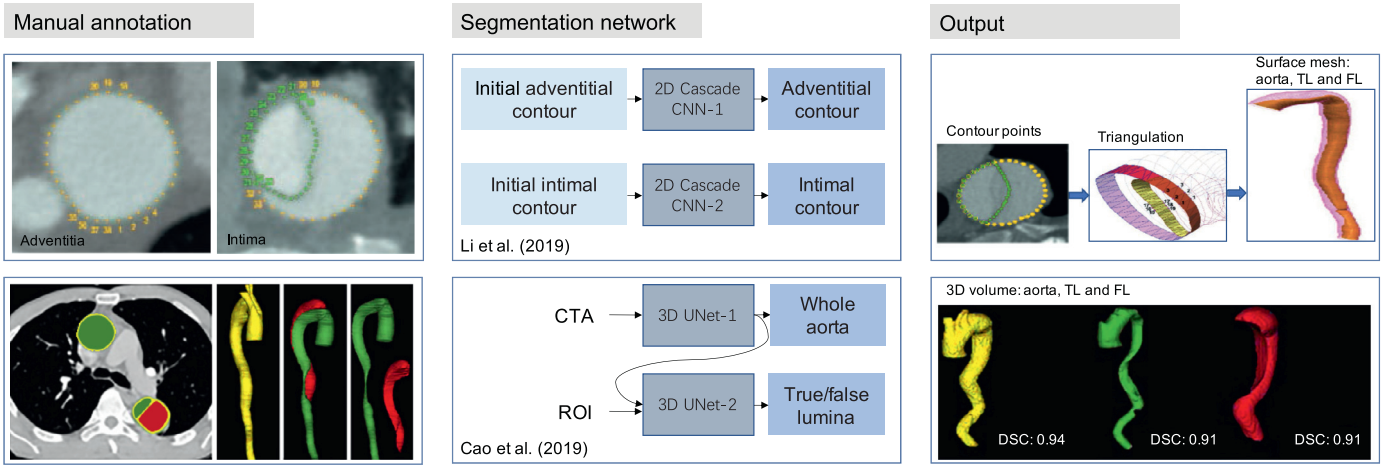

Fig. 10. Comparison of the two deep learning-based approaches with respect to data annotation, segmentation network and output from Li et al. (2019) (top row) and Cao et al. (2019) (bottom row). The first column, manual annotation, shows the type of annotation that the authors performed on their respective datasets. Li et al. (2019) annotated the contour of the overall aorta (yellow), i.e. approximately the shape of the adventitial layer, and the contour of the TL (green), i.e. approximately the shape of the intimal layer. Cao et al. (2019) performed a voxel-wise annotation of the TL (green), FL (red), and aortic wall with intimal flap (yellow). The second column, segmentation network, shows the operational workflow of both approaches. Li et al. (2019) provided initial contours which are refined by the CNNs, whereas Cao et al. (2019) introduced a two-step approach where first the overall aorta is segmented and afterwards a second CNN separates TL and FL. The second CNN, 3D UNet-2, only operates on a ROI defined by the output of the first CNN, 3D UNet-1. Finally, the third column, output, shows an example of the respective outputs as reported in the respective studies. The DSC (Dice similarity score) values refer to these reported in Cao et al. (2019). (For interpretation of the references to colour in this figure legend, the reader is referred to the web version of this article.)

learn the difference in the intensity distribution between the two lumina. However, the false lumen can be easily confused with the background as this has a similar intensity distribution to the background, especially in the presence of a thrombus. In other words, the mostly non-enhanced false lumen is more challenging to segment than the evenly enhanced true lumen if the training of the network is supervised by a mask, as in the work of Cao et al. (2019). The lower DSC values for false lumen segmentation are an evidence to this analysis. The disadvantage of mask-supervised training can be compensated by training the network using contours. However, a contour-supervised training can be affected by the artifacts caused by calcifications, as shown in Fig. 9 (bottom).

We therefore further propose that a combination of contour and region in the training process of deep learning networks will potentially increase the robustness of the networks and should be considered in future deep learning-based approaches for AD segmentation. Fig. 10 illustrates the comparison of the two approaches.

Note that both deep learning and classical methods do not provide a robust solution for the segmentation of thrombosed false lumina in the aorta and, potentially, in the branch arteries. As a starting point, we believe that this task could benefit from the existing literature on thrombus segmentation in aortic aneurysms (Lee et al. (2010); López-Linares et al. (2018)), given the similarity in the axial view. Furthermore, although some initial work on AD visualization has been performed (Mistelbauer et al. (2016); Burris et al. (2017)), more comprehensive visual analytics tools, which would allow not only an intra-patient but also an inter-patient analysis of the disease between geographic communities, are still missing.

5.3. Challenges ahead

Considering the fact that large, annotated and publicly available datasets such as ImageNet (Deng et al. (2009)) have greatly accelerated the advancement of computer vision, we believe that the development of future medical technology can also be driven by free, easy-accessible and expert-annotated medical datasets, which have already shown to be promising. In medical image segmentation (organs, tumors, etc.), state-of-the art results have been achieved by using deep learning-based approaches with publicly available datasets of various modalities and pathologies (Budai et al. (2013); Badrinarayanan et al. (2015); Wang et al. (2016); Pereira et al. (2016); Li et al. (2018); Blanc-Durand et al. (2018)). Some of them have already been integrated into the decision-making systems available in hospitals, providing benefits for the physicians (Bien et al. (2018); Hannun et al. (2018); De Fauw et al. (2018); Rajpurkar et al. (2018); Tang et al. (2019)).

Based on our investigation, computer-aided segmentation of ADs, i.e., the segmentation of the aorta and the true and false lumina, has been an under-investigated area and it lacks a clinically applicable system to help surgeons with the pre-operative planning for TEVAR surgery. As for other areas, large and annotated AD datasets could be the driving force for future advancements of AD segmentation approaches. An example is the BraTS data and segmentation collection (https://ieee-dataport.org/competitions/brats-miccai-brain-tumor-dataset), which has attracted many researchers developing and evaluating their algorithms. However, although initial work has been performed towards this direction, it can be expected that there is a long way to go before these datasets can be made publicly available. The difficulty in constructing an open access, large, and annotated AD dataset collection lies mainly in five aspects:

- AD is a rather rare disease and it is difficult for a single medical center to collect all the necessary AD cases in a short period of time
- AD annotation, i.e., the correct identification of true and false lumina requires expertise
- It is difficult to have a standardized annotation protocol that allows reproducible manual segmentation by different individuals as the identification of the boundary between the true lumen and the false lumen is subjective even for experienced radiologists and surgeons
- Lack of an easy-to-use annotation tool designed specifically for ADs. ITK-SNAP, 3D Slicer, MeVisLab, MITK and Studierfenster only allow slice-wise segmentation, which can be inefficient

- Medical data sharing, which requires the approval of an institutional review board, with strict data transmission rules, that has not been efficient among medical centers, academic institutions and the industry

Currently, hosting public challenges targeted at solving a specific healthcare problem has shown to be efficient in making medical datasets available to the public. Some well-known challenges are Grand Challenges (https://grand-challenge.org/challenges/), Kaggle Healthcare (https://www.kaggle.com/tags/healthcare/) and PhysioNet Challenges (https://physionet.org/challenge/), which are held in conjunction with conferences such as MICCAI (http://www.miccai.org/) and Computing in Cardiology (http://www.cinc.org/). These challenges are usually supported by industry partners, such as the Nvidia Corporation and have yielded many publications, state-of-the-art results and advanced the development of clinical technologies. Academic institutions such as the Stanford Machine Learning Group (https://stanfordmlgroup.github.io/) are also making efforts in data-sharing by hosting public challenges (Rajpurkar et al. (2017); Irvin et al. (2019)).

Besides the difficulty to construct an annotated AD database, the generalization performance of deep learning-based approaches for AD segmentations has not been fully addressed. As discussed in Section 3, traditional approaches can easily fail on AD cases with less common dissection morphology such as multi-barreled AD (AD with multiple false lumina). It is foreseeable that deep learning-based approaches will also fail when such cases are not included in the training set. This problem should be carefully addressed in future studies where deep learning is employed.

However, the different types and stages of ADs can also enable approaches to benefit from these specific characteristics. As we have seen, such prior knowledge has been exploited, e.g., by Kovács (2010) utilizing the prior knowledge of the circular shape of the aorta and the Hough transform. Furthermore, Kovács (2010) described how true and false lumina can be identified and segmented for TBAD (with the a priori assumption that the true lumen is connected to the non-dissected ascending aorta) and TAAD (with the a priori assumption that the false lumen has a larger cross-sectional area compared to the true lumen). As a fully automatic segmentation of 'general' ADs is very challenging and because they are categorized already in clinical practice, it makes sense using also a multi-stage approach, first dividing them into categories by training and applying a classifier. This can be two classes (Type A and B) according to the introduced Stanford classification, but also three classes (Type I, II and III) according to the DeBakey classification. Afterwards, use different segmentation methods that depend on the resulting AD class. These segmentation methods can make use of further anatomical knowledge, like organ locations (heart, liver), branches (to the kidney or carotid arteries) and common landmarks like the aortic arch.

5.4. Final remarks

Aortic dissection is a rare yet life-threatening disease and has been a major focus in clinical studies. However, the disease has been less intensively investigated by researchers from the fields of computer science and engineering, which makes the development pace of computer-aided AD diagnosis and treatment relatively slow. Computer-aided AD segmentation is the core step among the many AD management technologies such as AD detection, visualization, simulation and intimal tear detection. The improvement of these technologies rely, to a large extent, on improved AD segmentation algorithms; the AD segmentation papers were therefore defined as *core papers* in our review. A comprehensive and systematic analysis of existing AD segmentation approaches was conducted and we also provided well-founded sections on future directions and challenges ahead on the basis of our expertise in this field. Different from other review papers, which usually have more than 100 related studies, the number of related papers we included here is relatively small, due to the reason mentioned above. However, we believe that our review can provide a quick and comprehensive reference for computer scientists who want to contribute to accelerate the development of computer-aided management of ADs.

The contribution of our review is threefold. We

- provided an overview of current computer-aided AD management technologies where AD segmentation plays the key role,
- conducted a comprehensive introduction and comparison of existing AD segmentation algorithms, and gave a direction for future work on AD segmentation with a thorough analysis, and
- brought the attention of computer scientists to ADs, which has not yet been fully studied outside the medical field.

Declaration of Competing Interest

The authors declare that they have no known competing financial interests or personal relationships that could have appeared to influence the work reported in this paper.

CRediT authorship contribution statement

Antonio Pepe: Conceptualization, Methodology, Writing - original draft. **Jianning Li:** Conceptualization, Methodology, Writing - original draft. **Malte Rolf-Pissarczyk:** Writing - original draft. **Christina Gsaxner:** Writing - original draft. **Xiaojun Chen:** Supervision. **Gerhard A. Holzapfel:** Supervision, Writing - original draft. **Jan Egger:** Conceptualization, Methodology, Supervision.

Acknowledgments

We would like to thank the professional designer Zhaodi Deng for supporting us with the figure editing. We also thank Kathrin Bäumler and Dominik Fleischmann from Stanford University for sharing with us additional images related to their published study (Bäumler et al. (2020)). Further, we would like to acknowledge BioTechMed-Graz. This work received funding from the TU Graz Lead Project (Mechanics, Modeling and Simulation of Aortic Dissection), the Austrian Science Fund (FWF) KLI 678-B31: 'enFaced: Virtual and Augmented Reality Training and Navigation Module for 3D-Printed Facial Defect Reconstructions', and was supported by CAMed (COMET K-Project 871132), which is funded by the Austrian Federal Ministry of Transport, Innovation and Technology (BMVIT), the Austrian Federal Ministry for Digital and Economic Affairs (BMDW) and the Styrian Business Promotion Agency (SFG). Furthermore, the support of the National Natural Science Foundation of China (Grant Nos. 81971709, 81828003), the Foundation of Ministry of Education of China Science and Technology Development Center (Grant No. 2018C01038), and the Foundation of Science and Technology Commission of Shanghai Municipality (Grant No. 19510712200) is gratefully acknowledged. Finally, Antonio Pepe was supported by the Austrian Marshall Plan Foundation Scholarship n. 942121022222019 and Jan Egger was supported as visiting Professor by the Overseas Visiting Scholars Program from the Shanghai Jiao Tong University (SJTU) in China.

Supplementary material

Supplementary material associated with this article can be found, in the online version, at doi:10.1016/j.media.2020.101773.

References

Aktouf, Z., Bertrand, G., Perroton, L., 2002. A three-dimensional holes closing algorithm. Pattern Recognit. Lett. 23 (5), 523–531.

Alimohammadi, M., Bhattacharya-Ghosh, B., Seshadhri, S., Penrose, J.M.T., Agu, O., Balabani, S., Díaz-Zuccarini, V., 2014. Evaluation of the hemodynamic effectiveness of aortic dissection treatments via virtual stenting. Int. J. Artif. Org. 37, 753–762.

Badrinarayanan, V., Kendall, A., Cipolla, R., 2015. Segnet: a deep convolutional encoder-decoder architecture for image segmentation. IEEE Trans. Pattern Anal. Mach. Intell. 39, 2481–2495.

Bäumler, K., Vedula, V., Sailer, A.M., Seo, J., Chiu, P., Mistelbauer, G., Chan, F.P., Fischbein, M.P., Marsden, A.L., Fleischmann, D., 2020. Fluid–structure interaction simulations of patient-specific aortic dissection.. Biomech. Model. Mechanobiol., in press.

Bazilevs, Y., del Álamo, J.C., Humphrey, J.D., 2010. From imaging to prediction: emerging non-invasive methods in pediatric cardiology. Prog. Pediatr. Cardiol. 30 (1), 81–89.

Bazilevs, Y., Hsu, M.-C., Benson, D.J., Sankaran, S., Marsden, A.L., 2009. Computational fluid structure interaction: methods and application to a total cavopulmonary connection. Comput. Mech. 45, 77–89.

Behrens, T., Rohr, K., Stiehl, H.S., 2003. Robust segmentation of tubular structures in 3-D medical images by parametric object detection and tracking. IEEE Trans. Syst. Man. Cybernet. – Part B Cybernetics 33 (4), 554–561.

Bien, N., Rajpurkar, P., Ball, R.L., Irvin, J., Park, A., Jones, E., Bereket, M., Patel, B.N., Yeom, K.W., Shpanskaya, K.S., Halabi, S.S., Zucker, E.J., Fanton, G.S., Amanatullah, D.F., Beaulieu, C.F., Riley, G.M., Stewart, R.J., Blankenberg, F., Larson, D.B., Jones, R., Langlotz, C.P., Ng, A.Y., Lungren, M.P., 2018. Deep-learning-assisted diagnosis for knee magnetic resonance imaging: development and retrospective validation of MRNet. PLoS Med. 15 (11), e1002699.

Blanc-Durand, P., Gucht, A.V.D., Schaefer, N.G., Itti, E., Prior, J.O., 2018. Automatic lesion detection and segmentation of 18F-FET PET in gliomas: a full 3D U-Net convolutional neural network study. PloS One 13 (4), e0195798.

Bucurenciu, C., Costache, V., Cândea, G., 2019. Study of aortic dissections treatment. segmentation, simulation and valiadation of surgical results. In: MATEC Web of Conferences 290 (04004), pp. 1–8.

Budai, A., Bock, R., Maier, A., Hornegger, J., Michelson, G., 2013. Robust vessel segmentation in fundus images. Int. J. Biomed. Imag. 2013 (6), 154860.

Burris, N.S., Hoff, B.A., Kazerooni, E.A., Ross, B.D., 2017. Vascular deformation mapping (VDM) of thoracic aortic enlargement in aneurysmal disease and dissection. Tomography 3 (3), 163–173.

Cao, L., Shi, R., Ge, Y., Xing, L., Zuo, P., Jia, Y., Liu, J., He, Y., Wang, X., Luan, S., Chai, X., Guo, W., 2019. Fully automatic segmentation of type B aortic dissection from CTA images enabled by deep learning. Eur. J. Radiol. 121, 108713.

Chen, D., Müller-Eschner, M., von Tengg-Kobligk, H., Barber, D.C., Boeckler, D., Hose, R.D., Ventikos, Y., 2013. A patient-specific study of type-B aortic dissection: evaluation of true-false lumen blood exchange. Biomed. Eng. Online 12 (65), 1–16.

Codner, J.A., Lou, X., Duwayri, Y.M., Chen, E.P., Binongo, J.N., Moon, R., Jordan, W.D., Leshnower, B.G., 2019. The distance of the primary intimal tear from the left subclavian artery predicts aortic growth in uncomplicated type B aortic dissection. J. Vasc. Surg. 69 (3), 692–700.

Crosetto, P., Reymond, P., Deparis, S., Kontaxakis, D., Stergiopulos, N., Quarteroni, A., 2011. Fluid–structure interaction simulation of aortic blood flow. Comput. & Fluids 43 (1), 46–57.

Dake, M.D., Kato, N., Mitchell, R.S., Semba, C.P., Razavi, M.K., Shimono, T., Hirano, T., Takeda, K., Yada, I., Miller, D.C., 1999. Endovascular stent-graft placement for the treatment of acute aortic dissection. N. Engl. J. Med. 340 (20), 1546–1552.

De Fauw, J., Ledsam, J.R., Romera-Paredes, B., Nikolov, S., Tomasev, N., Blackwell, S., Askham, H., Glorot, X., O'Donoghue, B., Visentin, D., van den Driessche, G., Lakshminarayanan, B., Meyer, C., Mackinder, F., Bouton, S., Ayoub, K., Chopra, R., King, D., Karthikesalingam, A., Hughes, C.O., Raine, R., Hughes, J., Sim, D.A., Egan, C., Tufail, A., Montgomery, H., Hassabis, D., Rees, G., Back, T., Khaw, P.T., Suleyman, M., Cornebise, J., Keane, P.A., Ronneberger, O., 2018. Clinically applicable deep learning for diagnosis and referral in retinal disease. Nat. Med. 24, 1342–1350.

Dehghan, E., Wang, H., Syeda-Mahmood, T., 2017. Automatic detection of aortic dissection in contrast-enhanced CT. In: IEEE International Symposium on Biomedical Imaging, pp. 557–560.

Demertzis, S., Hurni, S., Stalder, M., Gahl, B., Herrmann, G., van den Berg, J.C., 2010. Aortic arch morphometry in living humans. J. Anat. 217 (5), 588–596.

Demos, T.C., Posniak, H.V., Churchill, R.J., 1986. Detection of the intimal flap of aortic dissection on unenhanced CT images. Am. J. Roentgenol. 146 (3), 601–603.

Deng, J., Dong, W., Socher, R., Li, L.-J., Li, K., Fei-Fei, L., 2009. ImageNet: a large-scale hierarchical image database. 2009 IEEE Conference on Computer Vision and Pattern Recognition 248–255.

Descoteaux, M., Audette, M., Chinzei, K., Siddiqi, K., 2005. Bone enhancement filtering: application to sinus bone segmentation and simulation of pituitary surgery. In: Duncan, J.S., Gerig, G. (Eds.), Medical Image Computing and Computer-Assisted Intervention Part I – MICCAI 2005. Springer, Berlin, Heidelberg, pp. 9–16.

Dotter, C.T., Roberts, D., Steinberg, I., 1950. Aortic length: angiocardiographic measurements. Circulation 2 (6), 915–920.

Duan, X., Shi, X., Wang, J., Chen, Q., 2018. Automatic aortic dissection recognition based on CT images. In: Proceedings of the 2nd International Conference on Biomedical Engineering and Bioinformatics (ICBEB), pp. 49–54.

Egger, J., Großkopf, S., Nimsky, C., Kapur, T., Freisleben, B., 2012. Modeling and visualization techniques for virtual stenting of aneurysms and stenoses. Computeriz. Med. Imag. Graph. 36 (3), 183–203.

Egger, J., Gunacker, S., Pepe, A., Melito, G.M., Gsaxner, C., Li, J., Ellermann, K., Chen, X., 2020. A comprehensive workflow and framework for immersive virtual endoscopy of dissected aortae from CTA data. In: Proceedings of SPIE Medical Imaging: Image-Guided Procedures, Robotic Interventions, and Modeling (11315), p. 1131531.

Eigen, K., Wels, M., Dohle, D., Suehling, M., Maier, A., 2018. Geometric modeling of the aortic inner and outer vessel wall from CTA for aortic dissection analysis. In: Proceedings of SPIE 10576, Medical Imaging 2018: Image-Guided Procedures, Robotic Interventions, and Modeling, pp. 105761X1–8.

Fetnaci, N., Lubniewski, P., Miguel, B., Lohou, C., 2013. 3D Segmentation of the true and false lumens on CT aortic dissection images. Proc. SPIE - Int. Soc. Opt. Eng. (4) 86500M1–15.

Gayhart, M., Arisawa, H., 2013. Automated detection of healthy and diseased aortae from images obtained by contrast-enhanced CT scan. Comput. Math. Methods Med. 2013 (26), 107871.

Gültekin, O., Hager, S.P., Dal, H., Holzapfel, G.A., 2019. Computational modeling of progressive damage and rupture in fibrous biological tissues: application to aortic dissection. Biomech. Model. Mechanobiol. 18, 1607–1628.

Hannun, A.Y., Rajpurkar, P., Haghpanahi, M., Tison, G.H., Bourn, C., Turakhia, M.P., Ng, A.Y., 2018. Cardiologist-level arrhythmia detection and classification in ambulatory electrocardiograms using a deep neural network. Nat. Med. 25, 65–69.

Harris, R.J., Kim, S., Lohr, J., Towey, S., Velichkovich, Z., Kabachenko, T., Driscoll, I., Baker, B., 2019. Classification of aortic dissection and rupture on post-contrast CT images using a convolutional neural network. J. Digit. Imag. 32 (6), 939–946.

He, K., Gkioxari, G., Dollár, P., Girshick, R.B., 2017. Mask R-CNN. 2017 IEEE Int. Conf. Comput. Vis. (ICCV) 2980–2988.

He, K., Zhang, X., Ren, S., Sun, J., 2015. Deep residual learning for image recognition. 2016 IEEE Conf. Comput. Vis. Pattern Recognit. (CVPR) 770–778.

de Hoon, N., van Pelt, R., Vilanova, A.J.A., 2014. 4D MRI Flow coupled to physics based fluid simulation for blood flow visualization. Comput. Graphics Forum 33 (3), 121–130.

Ho, D., Squelch, A., Sun, Z., 2017. Modelling of aortic aneurysm and aortic dissection through 3D printing. J. Med. Radiat. Sci. 64 (1), 10–17.

Huang, C.Y., Weng, S.H., Weng, C.F., Chen, W.Y., Chen, I.M., Hsu, C.P., Shih, C.C., 2013. Factors predictive of distal stent graft-induced new entry after hybrid arch elephant trunk repair with stainless steel-based device in aortic dissection. J. Trauma-Injury Infect. Crit. Care 146 (3), 623–630.

Huptas, S., Mehta, R.H., Kühl, H., Tsagakis, K., Reinsch, N., Kahlert, P., Jakob, H.G., Erbel, R., Eggebrecht, H., 2009. Aortic remodeling in type B aortic dissection: effects of endovascular stent-graft repair and medical treatment on true and false lumen volumes. J. Endovascul. Therapy 140 (3), 28–38.

Irvin, J., Rajpurkar, P., Ko, M., Yu, Y., Ciurea-Ilcus, S., Chute, C., Marklund, H., Haghgoo, B., Ball, R.L., Shpanskaya, K.S., Seekins, J., Mong, D.A., Halabi, S.S., Sandberg, J.K., Jones, R., Larson, D.B., Langlotz, C.P., Patel, B.N., Lungren, M.P., Ng, A.Y., 2019. CheXpert: a large chest radiograph dataset with uncertainty labels and expert comparison. In: The Thirty-Third AAAI Conference on Artificial Intelligence (AAAI-19), pp. 590–597.

Khan, I.A., Nair, C.K., 2002. Clinical, diagnostic, and management perspectives of aortic dissection. Chest 122 (1), 311–328.

Kim, K.M., Donayre, C.E., Reynolds, T.S., Kopchok, G.E., Walot, I., Chauvapun, J.P., White, R.A., 2011. Aortic remodeling, volumetric analysis, and clinical outcomes of endoluminal exclusion of acute complicated type B thoracic aortic dissections. J. Vasc. Surg. 54 (2), 316–325.

Kim, S.-J., Park, T.-H., Cho, Y.-R., Park, K., Park, J.-S., Kim, M.-H., Kim, Y.-D., 2019. Left ventricular geometric patterns in patients with type a aortic dissection. Cardiovasc. Ultrasound 17 (2), 1–5.

Kovács, T., 2010. Automatic segmentation of the vessel lumen from 3D CTA images of aortic dissection, 065. Dissertation. Hartung-Gorre Verlag, 1–127.

Kovács, T., Cattin, P., Alkadhi, H., Wildermuth, S., Székely, G., 2006a. Automatic segmentation of the aortic dissection membrane from 3D CTA images. In: International Conference on Medical Imaging and Augmented Reality. Springer, Berling, Heidelberg, pp. 317–324.

Kovács, T., Cattin, P., Alkadhi, H., Wildermuth, S., Székely, G., 2006b. Automatic segmentation of the vessel lumen from 3D CTA images of aortic dissection. Bildverarbeitung für die Medizin. Springer, Berlin, Heidelberg, pp. 161–165.

Krissian, K., Carreira, J.M., Esclarin, J., Maynar, M., 2014. Semi-automatic segmentation and detection of aorta dissection wall in MDCT angiography. Med. Image Anal. 18 (1), 83–102.

Krol, E., Panneton, J.M., 2017. Uncomplicated acute type B aortic dissection: selection guidelines for TEVAR. Annal. Vasc. Dis. 10 (3), 165–169.

Kurugol, S., Estepar, R.S.J., Ross, J., Washko, G.R., 2012. Aorta segmentation with a 3D level set approach and quantification of aortic calcifications in non-contrast chest CT. In: International Conference of the IEEE Engineering in Medicine and Biology Society, pp. 2343–2346.

Lauder, L., Ewen, S., Tzafriri, A., Edelman, E., Lüscher, T., Blankenstijn, P., Dörr, O., Schlaich, M., Sharif, F., Voskuil, M., Zeller, T., Ukena, C., Scheller, B., Böhm, M., Mahfoud, F., 2018. Renal artery anatomy assessed by quantitative analysis of selective renal angiography in 1,000 patients with hypertension. EuroIntervention 14 (1), 121–128.

Lee, K., Johnson, R.K., Yin, Y., Wahle, A., Olszewski, M.E., Scholz, T.D., Sonka, M., 2010. Three-dimensional thrombus segmentation in abdominal aortic aneurysms using graph search based on a triangular mesh. Comput. Biol. Med. 40 (3), 271–278.

Lee, N., Tek, H., Laine, A.F., 2008. True-false lumen segmentation of aortic dissection

using multi-scale wavelet analysis and generative-discriminative model matching. Proc. SPIE - Int. Soc.Opt. Eng. 6915, 69152V–69152V–11.
LeMaire, S.A., Russel, L., 2011. Epidemiology of thoracic aortic dissection. Nat. Rev. Cardiol. 8, 103–113.
Lesage, D., Angelini, E.D., Bloch, I., Gareth, F.L., 2009. A review of 3D vessel lumen segmentation techniques: models, features and extraction schemes. Med. Image Anal. 13 (6), 819–845.
Li, X., Chen, H., Qi, X., Dou, Q., Fu, C., Heng, P., 2018. H-DenseUnet: hybrid densely connected UNet for liver and tumor segmentation from CT volumes. IEEE Trans. Med. Imag. 37 (12), 2663–2674.
Li, Z., Feng, J., Feng, Z., An, Y., Gao, Y., Lu, B., Zhou, J., 2019. Lumen segmentation of aortic dissection with cascaded convolutional network. In: Pop, M., Sermesant, M., Zhao, J., Li, S., McLeod, K., Young, A., Rhode, K., Mansi, T. (Eds.), Statistical Atlases and Computational Models of the Heart. Atrial Segmentation and LV Quantification Challenges. Springer International Publishing, Cham, pp. 122–130.
Lohou, C., Fetnaci, N., Lubniewski, P., Miguel, B., Chabrot, P., Sarry, L., 2014. Intimai flap segmentation on CTA aortic dissection images based on mathematical morphology. In: International Conference on Biomedical Engineering and Informatics.
Lohou, C., Miguel, B., 2011. Detection of the aortic intimal tears by using 3D digital topology. Proc. SPIE - Int. Soc. Opt. Eng. 37 (4), 291–306.
Lu, Q., Feng, J., Zhou, J., Zhao, Z., Li, H., Teng, Z., Jing, Z., 2015. Endovascular repair by customized branched stent-graft: a promising treatment for chronic aortic dissection involving the arch branches. J. Thoracic Cardiovasc. Surg. 150 (6), 1631–1638.e5.
Lubniewski, P.J., Miguel, B., Sauvage, V., Lohou, C., 2012. Interactive 3D segmentation by tubular envelope model for the aorta treatment. Proc. SPIE - Int. Soc. Opt. Eng. 8290 (9), 841–845.
López-Linares, K., Aranjuelo, N., Kabongo, L., Maclair, G., Lete, N., Ceresa, M., García-Familiar, A., Macía, I., Ballester, M.A.G., 2018. Fully automatic detection and segmentation of abdominal aortic thrombus in post-operative CTA images using deep convolutional neural networks. Med. Image Anal. 46, 202–214.
Mao, S.S., Ahmadi, N., Shah, B., Beckmann, D., Chen, A., Ngo, L., Flores, F.R.V., Gao, Y.L., Budoff, M.J., 2008. Normal thoracic aorta diameter on cardiac computed tomography in healthy asymptomatic adults: impact of age and gender.. Acad. Radiol. 15 (7), 827–834.
Martínez-Mera, J.A., Tahoces, P.G., Carreira, J.M., 2013. A hybrid method based on level set and 3D region growing for segmentation of the thoracic aorta. Comput. Aid. Surg. 18 (5–6), 109–117.
Melissano, G., Bertoglio, L., Rinaldi, E., Civilini, E., Tshomba, Y., Kahlberg, A., Agricola, E., Chiesa, R., 2012. Volume changes in aortic true and false lumen after the 'PETTICOAT' procedure for type B aortic dissection. J. Vasc. Surg. 55 (3), 641–651.
Menichini, C., Cheng, Z., Gibbs, R.G., Xu, X.Y., 2016. Predicting false lumen thrombosis in patient-specific models of aortic dissection. J. R. Soc. Interface 13 (124), 1–11.
Menichini, C., Cheng, Z., Gibbs, R.G.J., Xu, X.Y., 2018. A computational model for false lumen thrombosis in type B aortic dissection following thoracic endovascular repair.. J. Biomech. 66, 36–43.
Milletari, F., Navab, N., Ahmadi, S.A., 2016. V-Net: fully convolutional neural networks for volumetric medical image segmentation. In: Fourth International Conference on 3D Vision, pp. 565–571.
Mistelbauer, G., Schmidt, J., Sailer, A., Bäumler, K., Walters, S., Fleischmann, D., 2016. Aortic dissection maps: comprehensive visualization of aortic dissections for risk assessment. In: VCBM '16: Proceedings of the Eurographics Workshop on Visual Computing for Biology and Medicine, pp. 143–152.
Morariu, C.A., Dohle, D.S., Terheiden, T., Tsagakis, K., Pauli, J., 2014. Polar-based aortic segmentation in 3D CTA dissection data using a piecewise constant curvature model. In: Bildverarbeitung für die Medizin, pp. 390–395.
Morariu, C.A., Dohle, D.S., Tsagakis, K., Pauli, J., 2015. Extraction of the aortic dissection membrane via spectral phase information. In: Bildverarbeitung für die Medizin, Informatik Aktuell, pp. 305–310.
Morariu, C.A., Huckfeldt, S.B., Dohle, D.S., Tsagakis, K., Pauli, J., 2016. A greedy completion algorithm for retrieving fuzzy fine structures. In: Bildverarbeitung für die Medizin, Informatik Aktuell, pp. 32–37.
Morariu, C.A., Terheiden, T., Dohle, D.S., Tsagakis, K., Pauli, J., 2014. Graph-based and variational minimization of statistical cost functionals for 3D segmentation of aortic dissections. In: German Conference on Pattern Recognition, Lecture Notes in Computer Science 8753, pp. 511–522.
Morariu, C.A., Terheiden, T., Dohle, D.S., Tsagakis, K., Pauli, J., 2016. Increasing the feasibility of minimally invasive procedures in type a aortic dissections: a framework for segmentation and quantification. Int. J. Comput. Assist. Radiol. Surg. 11 (2), 243.
Morariu, C.A., Zohourian, F., Dohle, D., Tsagakis, K., Pauli, J., 2016. Unsupervised extraction of the aortic dissection membrane based on a multiscale piecewise ridge model. In: IEEE International Symposium on Biomedical Imaging, pp. 305–310.
Nienaber, C.A., Clough, R.E., Sakalihasan, N., Suzuki, T., Gibbs, R., Mussa, F., Jenkins, M.P., Thompson, M.M., Evangelista, A., Yeh, J.S., Cheshire, N., Rosendahl, U., Pepper, J., 2016. Aortic dissection. Nature Revi. Dies. Primer. 21 (2), 16053.
Nienaber, C.A., Kische, S., Rousseau, H., Eggebrecht, H., Rehders, T.C., Kundt, G., Glass, A., Scheinert, D., Czerny, M., Kleinfeldt, T., Zipfel, B., Labrousse, L., et al., 2013. Endovascular repair of type B aortic dissection: long-term results of the randomized investigation of stent grafts in aortic dissection trial. Circulation: Cardiovascular Interventions 6 (4), 407–416.
Noothout, J., Vos, B.D., Wolterink, J., Isgum, I., 2018. Automatic segmentation of thoracic aorta segments in low-dose chest CT. In: Proceedings of SPIE Medical Imaging (10574), p. 105741S.
Olabarriaga, S.D., Rouet, J.-M., Fradkin, M., Breeuwer, M., Niessen, W.J., 2005. Segmentation of thrombus in abdominal aortic aneurysms from CTA with nonparametric statistical grey level appearance modeling. IEEE Trans. Med. Imag. 24 (4), 477–485.
Parmer, S.S., Carpenter, J.P., Stavropoulos, S.W., Fairman, R.M., Pochettino, A., Woo, E.Y., Moser, G.W., Bavaria, J.E., 2006. Endoleaks after endovascular repair of thoracic aortic aneurysms. J. Vasc. Surg. 44 (3), 447–452.
Paruchuri, V., Salhab, K.F., Kuzmik, G.A., Gubernikoff, G., Fang, H., Rizzo, J.A., Ziganshin, B.A., Elefteriades, J.A., 2015. Aortic size distribution in the general population: explaining the size paradox in aortic dissection. Cardiology 131 (4), 265–272.
Pereira, S., Pinto, A., Alves, V., Silva, C.A., 2016. Brain tumor segmentation using convolutional neural networks in MRI images. IEEE Trans. Med. Imag. 35 (5), 1240–1251.
Qi, Y., Ma, X., Li, G., Ma, X., Wang, Q., Yu, D., 2016. Three-dimensinal visualization and imaging of the entry tear and intimal flap of aortic dissection using CT virtual intravascular endoscopy. PLoS ONE 11 (10), e0164750.
Qiao, Y., Zeng, Y., Ding, Y., Fan, J., Luo, K., Zhu, T., 2019. Numerical simulation of two-phase non-newtonian blood flow with fluid-structure interaction in aortic dissection.. Comput. Methods Biomech. Biomed. Eng. 22 (6), 620–630.
Qing, K.-X., ki Yiu, W., Cheng, S.W., 2012. A morphologic study of chronic type B aortic dissections and aneurysms after thoracic endovascular stent grafting. J. Vasc. Surg. 55 (5), 1268–1276.
Rad, A.A., Faez, K., Qaragozlou, N., 2003. Fast circle detection using gradient pair vectors. In: Proceedings of the Seventh International Conference on Digital Image Computing: Techniques and Applications (DICTA), pp. 879–888.
Rajpurkar, P., Irvin, J., Bagul, A., Ding, D.Y., Duan, T., Mehta, H., Yang, B.J., Zhu, K., Laird, D., Ball, R.L., Langlotz, C.P., Shpanskaya, K.S., Lungren, M.P., Ng, A.Y., 2017. MURA: large dataset for abnormality detection in musculoskeletal radiographs. In: 1st Conference on Medical Imaging with Deep Learning (MIDL 2018), pp. 1–10.
Rajpurkar, P., Irvin, J., Ball, R.L., Zhu, K., Yang, B., Mehta, H., Duan, T., Ding, D.Y., Bagul, A., Langlotz, C.P., Patel, B.N., Yeom, K.W., Shpanskaya, K.S., Blankenberg, F., Seekins, J., Amrhein, T.J., Mong, D.A., Halabi, S.S., Zucker, E.J., Ng, A.Y., Lungren, M.P., 2018. Deep learning for chest radiograph diagnosis: a retrospective comparison of the CheXNeXt algorithm to practicing radiologists. PLoS Med. 15 (11), e1002686.
Rohlffs, F., Tsilimparis, N., Diener, H., Larena-Avellaneda, A., Von Kodolitsch, Y., Wipper, S., Debus, E.S., Koelbel, T., 2015. Chronic type B aortic dissection: indications and strategies for treatment. J. Cardiovasc. Surg. 56 (2), 231–238.
Ronneberger, O., Fischer, P., Brox, T., 2015. U-Net: convolutional networks for biomedical image segmentation. International Conference on Medical Image Computing and Computer-Assisted Intervention (MICCAI). LNCS, 9351. Springer, pp. 234–241.
Ryu, C.-W., Jahng, G.-H., Kim, E.-J., Choi, W.-S., Yang, D.-M., 2009. High resolution wall and lumen MRI of the middle cerebral arteries at 3 tesla.. Cerebrovasc. Dis. 27 (5), 433–442.
Schoder, M., Czerny, M., Cejna, M., Rand, T., Stadler, A., Sodeck, G., Gottardi, R., Loewe, C., Lammer, J., 2007. Endovascular repair of acute type B aortic dissection: long-term follow-up of true and false lumen diameter changes. Ann. Thoracic Surg. 83 (3), 1059–1066.
Seada, N., Hamad, S., Mostafa, M.G., 2016. Model-based automatic segmentation of ascending aorta from multimodality medical data. Int. J. Electric. Comput. Eng. 6 (6), 3161–3173.
Seada, N.A., Hamad, S., Mostafa, M.G.M., 2016. Automatically seeded region growing approach for automatic segmentation of ascending aorta. In: Proceedings of the 10th International Conference on Informatics and Systems, pp. 127–132.
Sherifova, S., Holzapfel, G.A., 2019. Biomechanics of aortic wall failure with a focus on dissection and aneurysm: a review. Acta Biomater. 99 (2019), 1–17.
Shorten, C., Khoshgoftaar, T.M., 2019. A survey on image data augmentation for deep learning. J. Big Data 6 (60), 1–48.
Stanley, G.A., Murphy, E.H., Knowles, M., Ilves, M., Jessen, M.E., Dimaio, M., Modrall, G., Arko 3rd, F.R., 2011. Volumetric analysis of type b aortic dissections treated with thoracic endovascular aortic repair. J. Vasc. Surg. 54 (4), 985–992.
Szpinda, M., Szpinda, A., WoŸniak, A., Daroszewski, M., Mila-Kierzenkowska, C., 2012. The normal growth of the common iliac arteries in human fetuses — an anatomical, digital and statistical study. Med. Sci. Monitor 18 (3), BR109–BR116.
Tang, H., Chen, X., Liu, Y., Lu, Z., You, J., Yang, M., Yao, S., Zhao, G., Xu, Y., Chen, T., Liu, Y., Xie, X., 2019. Clinically applicable deep learning framework for organs at risk delineation in CT images. Nature Mach. Intell. 1, 480–491.
Tek, H., Ayvaci, A., Comaniciu, D., 2005. Multi-scale vessel boundary detection. In: Computer Vision for Biomedical Image Applications. LNCS 3765, pp. 388–398.
Thubrikar, M.J., Agali, P., Robicsek, F., 1991. Wall stress as a possible mechanism for the development of transverse intimal tears in aortic dissections. J. Med. Eng. Technol. 23 (4), 127–134.
Trullo, R., Petitjean, C., Ruan, S., Dubray, B., Nie, D., Shen, D., 2017. Segmentation of organs at risk in thoracic CT images using a SharpMask architecture and conditional random fields. In: Proceedings of IEEE International Symposium on Biomedical Imaging, pp. 1003–1006.
Tsai, T.T., et al., 2007. Partial thrombosis of the false lumen in patients with acute type b aortic dissection. New Engl. J. Med. 357, 349–359.
Vitanovski, D., Ralovich, K., Ionasec, R., Zheng, Y., Suehling, M., Krawtschuk, W.,

Hornegger, J., Comaniciu, D., 2012. Personalized learning-based segmentation of thoracic aorta and main branches for diagnosis and treatment planning. In: IEEE International Symposium on Biomedical Imaging, pp. 836–839.
Wang, G.J., Fairman, R.M., 2009. Endovascular repair of the thoracic aorta. Semin. Intervent. Radiol. 26 (1), 17–24.
Wang, J., Mackenzie, J.D., Ramachandran, R., Chen, D.Z., 2016. A deep learning approach for semantic segmentation in histology tissue images. In: Medical Image Computing and Computer-Assisted Intervention (MICCAI). LNCS 9901, pp. 176–184.
Wong, S.C., Gatt, A., Stamatescu, V., McDonnell, M.D., 2016. Understanding data augmentation for classification: when to warp? 2016 Int. Conf. Digit. Image Comput. 1–6.
Xiaojie, D., Meichen, S., Jianming, W., He, Z., Dandan, C., 2016. Segmentation of the aortic dissection from CT images based on spatial continuity prior model. In: 2016 8th IEEE International Conference on Information Technology in Medicine and Education (ITME), pp. 275–280.
Xie, Y., Padgett, J., Biancardi, A., Reeves, A., 2014. Automated aorta segmentation in low-dose chest CT images. Int. J. Comput. Assist. Radiol. Surg. 9 (2), 211–219.
Xu, X., He, Z., Niu, K., Zhang, Y., Tang, H., Tan, L., 2019. An automatic detection scheme of acute Stanford type A aortic dissection based on DCNNs in CTA images. In: ICMSSP 2019: Proceedings of the 2019 4th International Conference on Multimedia Systems and Signal Processing, pp. 16–20.
Yi, X., Walia, E., Babyn, P., 2019. Generative adversarial network in medical imaging: areview. Med. Image Anal. 58 (101552), 1–20.

SUPPLEMENTARY MATERIAL

Flow Diagram

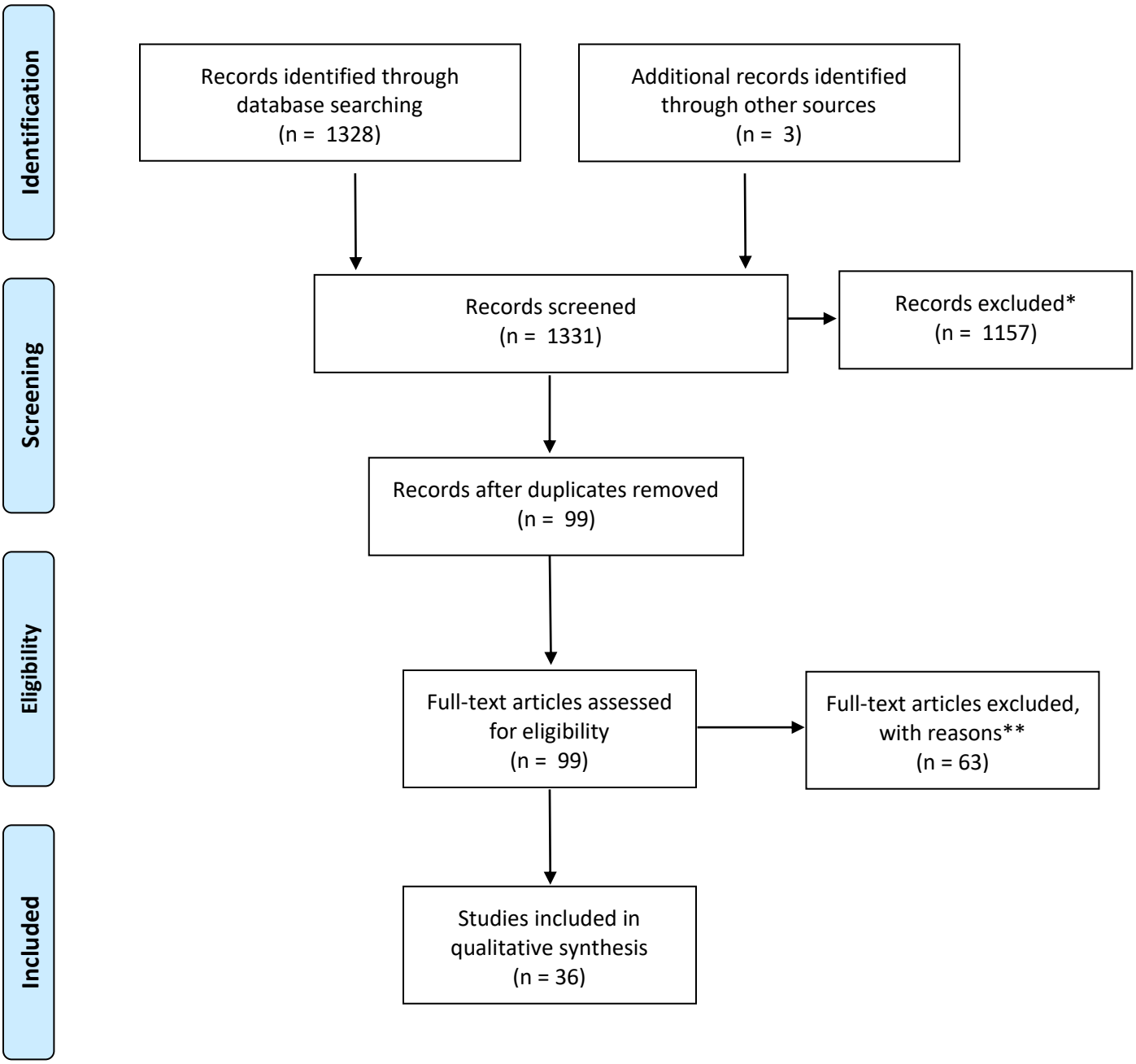

*The reason for exclusion was the solely clinical relevance of the article or the usage of the term 'aortic dissection' to simply enumerate the possible pathologies of the aorta.
** The reason for exclusion was the high similarity with other articles, e.g., the same approach has a more in-depth coverage in one or more other articles. Another common reason was the inclusion of the term 'aortic dissection' in the motivation, although the results were only shown for images of healthy patients.

Original source: Moher D, Liberati A, Tetzlaff J, Altman DG, The PRISMA Group (2009). Preferred reporting items for systematic reviews and meta-analyses: the PRISMA statement. PLoS Medicine 6(7): e1000097.

SEARCH ENGINES:
IEEE Xplore, PubMed, Google Scholar, Scopus, DBLP

Keywords:
‘aortic dissection’ AND {‘segmentation’, ‘detection’, ‘visualization’, ‘geometry’, ‘mesh’}

Date of search: October 2019

Searches:

‘aortic dissection’ AND ‘detection’:
IEEE Xplore: 7
PubMed: 302
Google Scholar°: 470
Scopus^: 22
DBLP: 2
TOTAL: 803

‘aortic dissection’ AND ‘segmentation’:
IEEE Xplore: 10
PubMed: 8
Google Scholar°: 65
Scopus^: 46
DBLP: 10
TOTAL: 139

‘aortic dissection’ AND ‘visualization’:
IEEE Xplore: 1
PubMed: 94
Google Scholar°: 107
Scopus^: 20
DBLP: 1
TOTAL: 223

‘aortic dissection’ AND (‘geometry’ OR ‘mesh’):
IEEE Xplore: 8
PubMed: 78
Google Scholar°: 17
Scopus^: 60
DBLP: 0
TOTAL: 163

TOTAL: 1328
° Differently than other engines, Google Scholar also searches in text and references. Therefore, only in this specific case, each search was filtered with the operator ‘intitle’, e.g., ‘aortic dissection’ AND intitle:‘detection’.
^ In the filtering options the different fields of ‘Computer Science’, ‘Mathematics’, ‘Multidisciplinary’, ‘Physics’, ‘Material Sciences’, ‘Engineering’ have been selected.

DATABASE OVERLAP

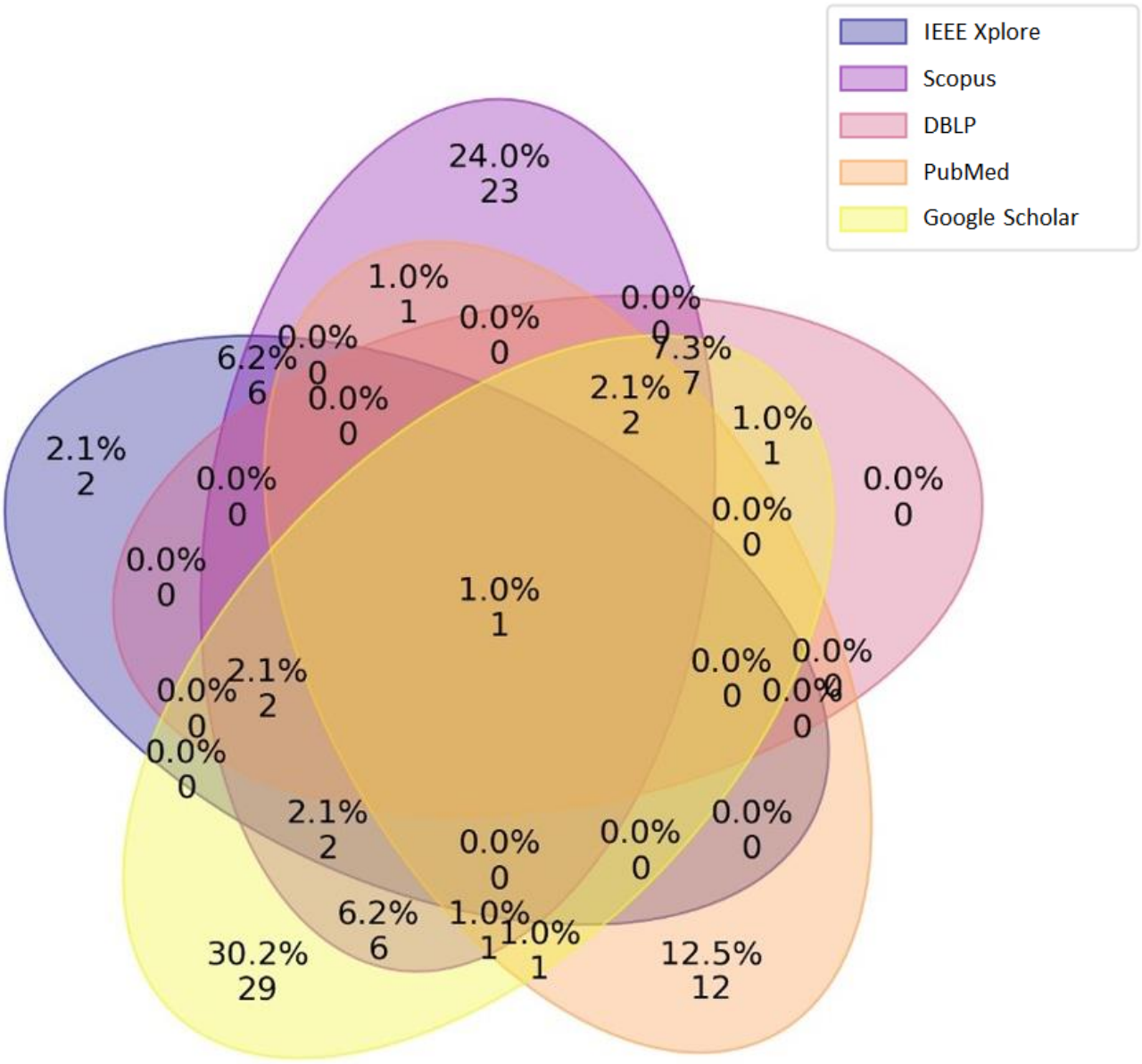

1 – Overall distribution after screening of the articles retrieved from the five databases and relative overlapping.

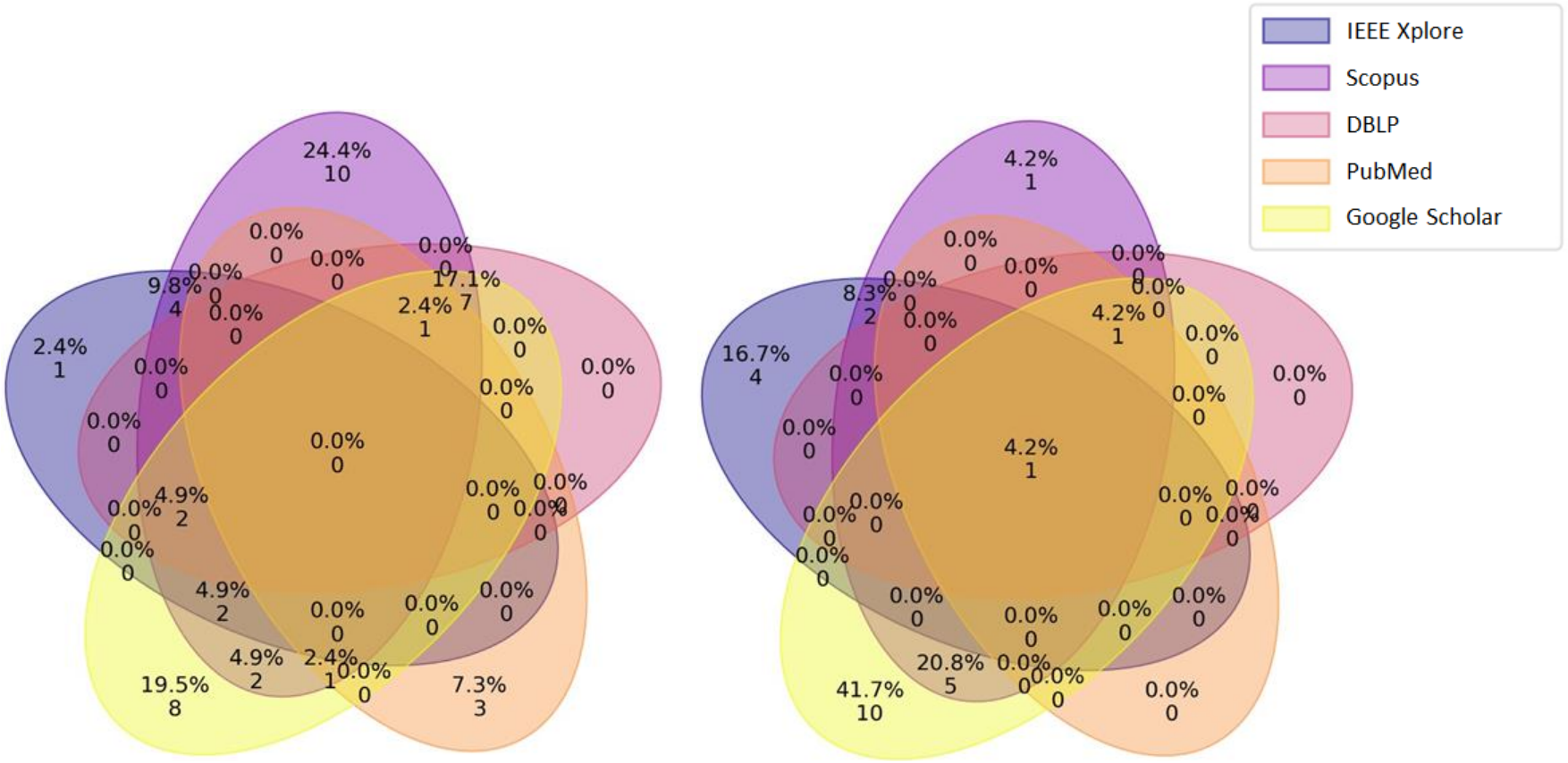

2 - Overlap of the screened papers between the different databases grouped by search keywords:
left: *'aortic dissection'* AND ***'segmentation'***,
right: *'aortic dissection'* AND ***'detection'***.

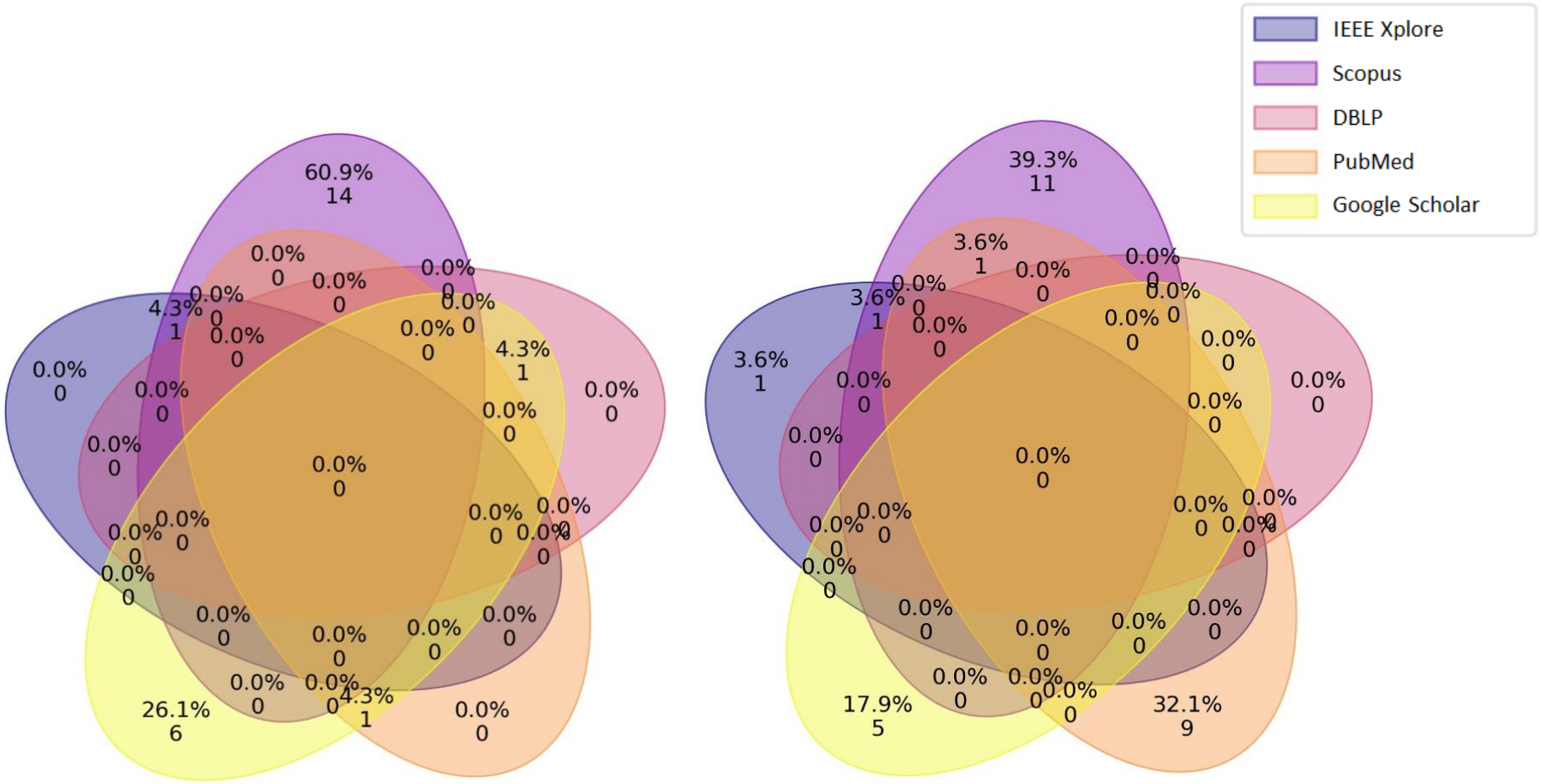

3 - Overlap of the screened papers between the different databases grouped by search keywords:
left: *'aortic dissection'* AND ***'visualization'***,
right: *'aortic dissection'* AND (***'geometry'*** OR ***'mesh'***).